ILAR Journal, 2018, 1–19

doi: 10.1093/ilar/ily010
Review Article

In Vivo Imaging With Confirmation by Histopathology for Increased Rigor and Reproducibility in Translational Research: A Review of Examples, Options, and Resources

Kathleen Gabrielson[1], Robert Maronpot[2], Sébastien Monette[3], Coraline Mlynarczyk[4], Yuval Ramot[5], Abraham Nyska[6], and Polina Sysa-Shah[7]

[1]Departments of Molecular and Comparative Pathology and Pathology School of Medicine, Environmental Health Engineering Bloomberg School of Public Health, Johns Hopkins University, Baltimore, Maryland, [2]Maronpot Consulting LLC, Raleigh, North Carolina, [3]Laboratory of Comparative Pathology, Memorial Sloan Kettering Cancer Center, The Rockefeller University, Weill Cornell Medicine, New York, New York, [4]Department of Medicine, Division of Hematology & Medical Oncology and the Meyer Cancer Center, Weill Cornell Medicine, New York, New York, [5]Department of Dermatology, Hadassah—Hebrew University Medical Center, Kiryat Hadassah, Jerusalem, Israel, [6]Sackler School of Medicine, Tel Aviv University, Tel Aviv, Israel and Toxicologic Pathology, Timrat, Israel, and [7]Department of Radiology, Miller Research Building Molecular Imaging Service Center, Johns Hopkins University, Baltimore, Maryland

Address correspondence and reprint requests to Kathleen Gabrielson, DVM, PhD, DACVP, Departments of Molecular and Comparative Pathology and Pathology School of Medicine, Environmental Health Engineering Bloomberg School of Public Health, Johns Hopkins University, 733 North Broadway, Miller Research Building, Room 807, Baltimore, Maryland 21205-2196. E-mail: kgabriel@jhmi.edu.

Abstract

Preclinical noninvasive imaging can be an indispensable tool for studying animal models of disease. In vivo imaging to assess anatomical, functional, and molecular features requires verification by a comparison to the macroscopic and microscopic morphological features, since all noninvasive in vivo imaging methods have much lower resolution than standard histopathology. Comprehensive pathological evaluation of the animal model is underutilized; yet, many institutions have veterinary or human pathologists with necessary comparative pathology expertise. By performing a rigorous comparison to gross or histopathology for image interpretation, these trained individuals can assist scientists with the development of the animal model, experimental design, and evaluation of the in vivo imaging data. These imaging and pathology corroboration studies undoubtedly increase scientific rigor and reproducibility in descriptive and hypothesis-driven research. A review of case examples including ultrasound, nuclear, optical, and MRI is provided to illustrate how a wide range of imaging modalities data can be confirmed by gross or microscopic pathology. This image confirmation and authentication will improve characterization of the model and may contribute to decreasing costs and number of animals used and to more rapid translation from preclinical animal model to the clinic.

Key words: CT; gross and histopathology; MRI; optical imaging; PET and SPECT; preclinical imaging; rigor and reproducibility; ultrasound imaging

Introduction

More than 2 decades ago, advancements in clinical imaging widened the possibilities for preclinical imaging methodologies leading to equipment and method development for assessment of smaller animal species. New systems were created to specifically image these species with the increased resolution necessary to answer research questions. Designed for zebrafish, rodents, and rabbits, these new systems for ultrasound, magnetic resonance, optical, and nuclear imaging systems now accommodate the needs of researchers to capture images on par with human imaging equipment resolution. For example, equipment designed specifically for rodent MRI incorporates magnet strengths from 9.4 to 11.2 Tesla into miniaturized systems that allow for improved resolution. In comparison, human clinical MRI scanners have magnets that range between 2 and 4 Tesla for practical clinical resolution of larger human organs. In a second example, the 3-chambered heart of the zebrafish can be evaluated by ultrasound using a recently developed high-frequency transducer at 50 to 70 MHz, while in comparison, transducers to evaluate the 4-chambered human heart require 2.5 to 5 MHz transducers for similar resolution.

One of the most beneficial aspects of noninvasive imaging is the application for serial imaging over time. This feature reduces the number of animals needed for a complete study since a disease process can be evaluated at multiple time points. Noninvasive imaging allows an animal to serve as a pretreatment control before treatment begins. Longitudinal imaging of the same animal will increase the data sensitivity as inter-individual variation in phenotype invariably occurs, even in inbred rodents. Observing the animal over multiple time points is key to documenting the progression of a disease and determining when it is necessary to kill animals to collect organ and tissue samples at the most accurate endpoint representative of the disease stage of interest. This feature prevents unexpected deaths as some animals may mask their symptoms. In addition, upon treatment with experimental drugs, animals may respond differently, and each animal may have an individual timeline for development of drug effects. The use of longitudinal in vivo imaging is an integral part of the refinements that have been introduced to improve the translational values of mouse models of cancer and other disease states.

Noninvasive imaging methods that offer molecular imaging, such as nuclear and optical modalities, allow for the utility of highly specific bioactive molecules such as radioactive or optical tracers that bind to specific targets in live animals and monitor molecular functional changes. Further, it is an advantage to perform functional dynamic studies in the same animal, recording minute-to-minute changes induced by experimental drug administration in real time. Most dual-imaging systems offer anatomy-oriented imaging features such as CT and MRI, which are included for sufficient anatomical detail for nuclear neuroimaging[1] or nuclear imaging for cancer studies.[2] Attention should be paid to the differences in anatomical/positional terminology when comparing preclinical and clinical anatomical studies.[3]

Most imaging methods require anesthesia as motion of the animal causes artifacts in the image. The investigator chooses between inhalation (eg, isoflurane) and injection (eg, ketamine/xylazine) anesthetic agents, considering several factors, including ease of administration (inhalable agents require anesthesia system and tubing arranged to reach the animal on the imaging bed) and effects on physiological parameters of the animal. Some systems have a gated acquisition to only acquire an image between respirations or in a specific phase of the cardiac cycle. There has been much progress in the development of equipment capable of obtaining images in unanesthetized animals. To accomplish this, animals have detectable reference points placed on their skull that allow for a strategy to triangulate the animal's position within the imaging system, and this information is used in the reconstruction of images. Currently, ultrasound is the only method that does not always require anesthesia. Within seconds to minutes, the ultrasound investigator can be informed of the physiology or function of an organ even in an awake animal habituated to the procedure. For example, as the mouse is held securely, the heart structure can be immediately visualized, images captured, stored, and at a later time these images can be analyzed to determine wall thickness or the dimensions of the left ventricle in diastole or systole. Although anesthesia typically causes heart rate reduction, observing the strength and magnitude of heart contractions in real time can be crucial in determining whether an animal should be killed due to heart failure thus supporting the 3Rs (refinement, reduction, and replacement) related to animal use in research.

In vivo imaging is applicable across multiple organ systems, disease types, and species. Each imaging modality has advantages and disadvantages outlined in Table 1. Using key words (in vivo, imaging animals) more than 40 000 publications in PubMed document the rich resource for imaging applications and protocols. Other publications regarding in vivo imaging offer alternative case examples and resources to be examined.[4–8]

While in vivo imaging has become increasingly sophisticated and has provided new opportunities to leverage preclinical models for translational research, applying rigor in their use is essential to ensure valid and reproducible results. Many of the publications do not provide histological endorsement of imaging data, while such a comparison would add to the credibility of the findings reported. For example, supplementing the positron emission tomography (PET) finding of metastasis in a rodent model of cancer with histological characterization of the tumors would enhance the scientific and translational value of the data. Without verification by other methods, there is a risk that in vivo imaging results may be misinterpreted. Gross and microscopic evaluation by pathologists with expertise in animal models, when performed with close collaboration with scientists using in vivo imaging, presents a unique opportunity for ultimate validation of in vivo imaging data. The purpose of the present review is to draw parallels and give examples of imaging-to-pathology correlations in multiple species

Table 1 A comparison between the advantages and disadvantages of each in vivo imaging method

	Ultrasound	PET/SPECT	CT/faxitron	Optical	MRI
Modality physics	Sound waves	Radioactivity	X-ray	Light fluorescence	Magnetic field
Noninvasive (survival)	√	√	√	√	√
Longitudinal	√	√	√	√	√
Reduction of animals	√	√	√	√	√
Quantitative	√	√	√	√	√
Structure	√	√	√	√	√
Function	√	√	√	√	√
Sensitivity	μM-mM	fM	μM	pM to fM (depth limits)	μM-mM
Gene expression	√	√	√	√	√
Resolution estimation	0.03 mm	1 mm PET 0.250 mm 3D SPECT	0.05 mm	0.250 mm	0.05 mm
Imaging time	minutes	10–60 minutes	minutes	minutes	30–60 minutes
Anesthesia	sometimes	√	√	√	√
Cost	+	+++	++	+	++++
Translational to humans	√	√	√	√	√

where in vivo imaging was used to document anatomical, functional, and molecular features in an animal model of disease, and to show how in vivo imaging and pathology, when performed concurrently, can provide precise and reproducible assessment of models at a level that could not be achieved by either method alone.

Ultrasound Imaging

Background

Ultrasound imaging is one of the earliest developed, safest, and least expensive modalities used clinically for decades in human and veterinary medicine. Clinical ultrasound machines have been adapted specifically for rodents notably (VisualSonics machines) and are widely available. Ultrasound imaging utilizes the differences of sound wave propagation and reflection off of solid, liquid, and gaseous matter in the body. Sound waves of defined frequencies generated by a transducer (or probe) travel through the body and are reflected back and returned to the transducer as reflected echoes. These echos are then converted into electrical signals and further processed to generate a 2D still image or a movie that one can observe in real time or at a later time. Ultrasound waves are reflected at the borders between tissues of different densities. The higher the difference between densities of tissues, the higher proportion of the waves reflected back to the transducer. At higher frequencies (50–70 MHz), the resolution increases, while the penetration depth of the sound wave decreases. High-frequency probes have been developed for rodents and zebrafish and have remarkable resolution of the fish heart[9] or for mouse embryos.[10–12]

Ultrasound methods evaluate anatomy, function, endothelial molecular changes, and blood flow through organs. Advanced ultrasound methods had been developed for ocular imaging,[13] intravascular imaging, and living mouse embryo imaging used for microinjections into the embryo.[14] Introduction of gas-filled microbubbles into the blood helps to better visualize blood flow through organs,[15] this technique had been used in embryos[16,17] while microbubbles conjugated to antibodies (ie, antibodies against endothelial cell surface proteins) allow imaging and quantification of molecular targets such as (VEGFR2) on endothelium and show the extent of blood vessels[18] in an organ or tumor. Another modality based on the usage of ultrasound waves is photoacoustic (PA) imaging, which relies on nonionizing laser pulses delivered to the studied tissues and registration and analysis of the produced acoustic waves. Ultrasound has been recently combined with the PA imaging modality to provide anatomical information for the functional PA data, such as oxygen saturation in blood.[19]

Advantages

Ultrasound systems generally are less expensive compared with other imaging systems, are portable (wheeled or carried), and require less maintenance. Except for the contrast and microbubble ultrasound methods,[20–22] no tracers or injectable agents are required. Other advantages include safety, good resolution (up to 30 microns), and the ability to obtain both anatomical and real-time functional data rapidly without image reconstruction. Molecular data regarding vasculature are also a feature measured by ultrasound and have been applied to cancer and inflammation research.[23–25] Easy to operate, these systems require skills that are obtainable through short courses, online instructional videos, and imaging skill mentors.

Limitations

Poor visualization of bone-obscured organs (brain) is observed unless openings are made into the skull to allow access of sound waves. Limited depth penetration is present with high-frequency sound waves.

Small vs Large Animal Ultrasound Imaging

Ultrasound systems developed for human patients are easily used for large animals. Portable ultrasound systems are very useful for ruminant, swine, and equine application in the field. Multiple laboratory animals including nonhuman primates in research and zoological collections[26] are imaged by ultrasound. High-resolution systems specifically developed for small rodents allow functional cardiovascular imaging in small animals[27] where the high heart rate can exceed 700 beats per minute. Awake mice are easily monitored with ultrasound systems with suitable high frame rates up to 1000 frames per second.[28] In anesthetized rodents, ECG monitoring can allow synchronization with echocardiography data to allow for more sophisticated speckle-tracking-based strain analysis.[29–31] Speckle-tracking-based strain analysis is one of the relatively novel ultrasound techniques based on evaluation of spotty acoustic phenomena ("speckles") observed during ultrasound visualization of cardiac tissue, which are unique for each cardiac region and consistent from frame to frame, thus allowing "tracking" of the

changes in the moving heart and, after postprocessing, to make conclusions about movement deformations ("strain") of cardiac tissue.

Comparison of Ultrasound Imaging to Pathology

One of the advantages of ultrasound imaging relates to the ability of the user to quickly determine the physiologic state of an animal for the selection of the experimental timing. For example, ultrasound can assist in determining the presence of early pregnancy in mice. When breeding a group of mice in an overnight (timed) 12-hour period, approximately 20% will become pregnant. If the investigational team requires to use only pregnant mice at a certain stage of pregnancy for their studies, ultrasound imaging can be used quickly (seconds) and inexpensively to determine the mice that are pregnant, excluding those not pregnant that could be used for rebreeding. Mouse weights can be used to determine pregnancy as well as abdominal palpation or tracking changes in steroid hormones, but these methods are not 100% accurate, particularly before day 7.5 of gestation.[32,33] Ultrasound imaging can visually determine a viable pregnancy at 8.5 days of pregnancy as seen in Figure 1 and as early as day 4.5.[34]

In a second example, ultrasound is used to determine aortic enlargement before aortic aneurism and dissection occur in a mouse model of Marfan disease. Marfan disease is a systemic disorder of connective tissue, characterized by skeletal, eye, and lung pathology and cardiac complications such as aortic dissection and mitral valve prolapse and dysfunction.[35] Mice with the fibrillin-1 gene mutation, found in Marfan disease, have cardiovascular disease phenotypes similar with humans and have been studied carefully using ultrasound to understand the mechanisms of disease progression (Figure 2). Ultrasound can also be used to determine atrioventricular (mitral) valve prolapse in these mice, and 2D images are used to quantify aortic diameters. This imaging information led to determining specific aberrant signaling pathways important in the progression of the Marfan's cardiovascular phenotype.[35,36] Imaging hundreds of mice under different treatments allowed these investigators to determined that TGFβ was dysregulated in this genetic disease. This discovery lead to clinical trials in Marfan patients with drugs that inactivated these pathways (Losartan) (NCT00593710, NCT00763893, NCT00723801, NCT01145612). Currently, newly diagnosed patients are surviving this deadly disease due to the new treatments monitored by ultrasound imaging studies. If ultrasound had not been available to these researchers, thousands of mice would have been studied in multiple treatment groups and killed at multiple time points to determine by pathology which drugs were effectively blocking disease progression. Indispensable ultrasound of these mice reduced the time for the discovery of novel treatments for Marfan disease, saving human lives.

Summary

Ultrasound imaging is inexpensive, relatively easy to learn and interpret, and available at most research institutions. Although

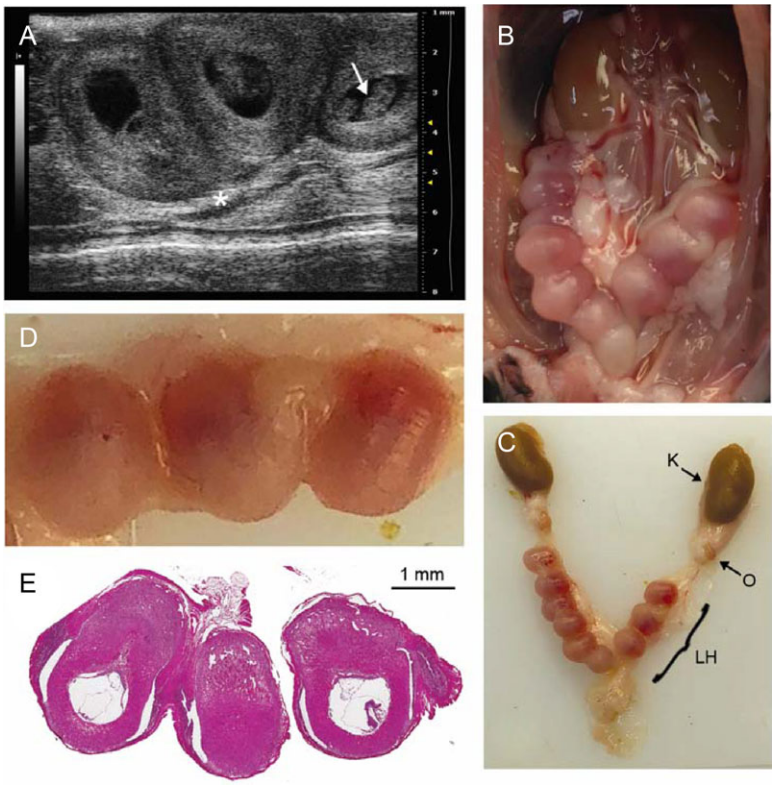

Figure 1 High-frequency ultrasound imaging of mouse uterus (E8.5 pregnancy) with pathology verification. (A) Ultrasound imaging was performed in wild-type mouse 8.5 days after a 12-hour overnight timed breeding. High frequency 50- to 70-mHz transducer was utilized to gain resolution to detect pregnancy. The lower abdomen 2-dimensional (2D) image shows the thickened wall uterus (asterisk) with placentation and the 3 implantation sites with developing fetuses. The hypoechoic area is due to fluid in the amniotic sac and appears black on the image. One fetus is labeled (white arrow). (B) Mouse was killed and the uterus was photographed in situ in the lower abdomen. (C) Dissected uterus with attaching kidneys and ovaries. (E) Microscopic view of 3 conceptuses. (D) Close up of 3 conceptuses within uterus. K, kidney; LH, left horn (uterus); O, ovary. (unpublished data).

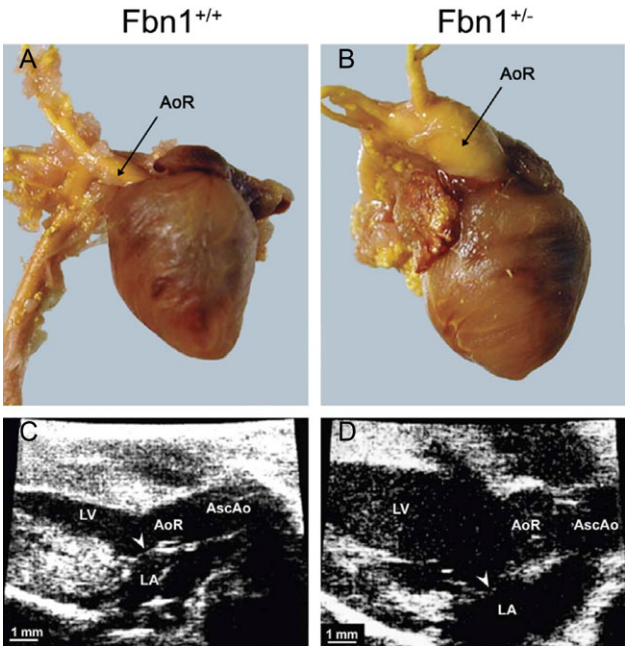

Figure 2 Comparison of gross morphology to 2-dimensional (2D) ultrasound imaging in a murine model of Marfan syndrome (fibrillin-1 [Fbn1]-deficient mice vs wild-type mice). The advantage of ultrasound imaging assisted the investigators in demonstrating drug efficacy to prevent aortic rupture in Marfan mouse model. Gross pathology of hearts from wild-type mice (A) compared with Fbn1 C1039G/+ animals (B) is compared with 2D ultrasound images of wild type (C) and Fbn1 C1039G/+ (D). AoR, aorta root; AscAo, ascending aorta; LA, left atrium; LV, left ventricle. Maronpot et al. with permission.[6]

used mostly in monitoring the heart structure and function or tumor size and vascularity, embryonic developmental studies have also benefited from this noninvasive modality. Noninvasive longitudinal ultrasound imaging allows for an animal model to be followed as the disease progresses with or without intervention. This in turn allows for selection of humane time points for euthanasia. Anesthesia is not always needed to acquire images, and this feature can allow for higher animal throughput with less manipulation of the animal. For example, in monitoring cardiovascular disease, anesthesia reduces heart rate and cardiac function and thus it can mask differences in a cardiovascular disease phenotype when comparing animals.[37] When possible, habituating the animals to the handling of ultrasound without anesthesia would produce more reliable experimental data. The comparison of ultrasound findings with higher resolution microscopy compliments and supports the ultrasound imaging data to ultimately improve research outcomes and translational relevance.

Nuclear Imaging

Background

Two main nuclear medicine imaging modalities are available for preclinical imaging, PET,[38,39] and single photon emission computed tomography (SPECT).[40] PET imaging employs positron-emitting radioisotopes, the most common of which is ^{18}F (with a half-life of 109 minutes). The most common radiotracer is ^{18}F-FDG, which is a glucose analog with a hydroxyl group substituted with ^{18}F. In using ^{18}F-FDG as a radiotracer in oncology preclinical studies, the supposition is that the metabolic demands of the cancer cells exceed that of normal cells so that ^{18}F-glucose will preferentially localize in the cancer cells (vs normal cells), allowing detection with PET imaging. In addition to ^{18}F-FDG, another example of ^{18}F-based tracer is fluoro-DOPA used to study dopaminergic pathways. Custom-made ^{18}F-labeled antibodies have been used to target specific proteins of interest. ^{11}C, ^{64}Cu, and other radioisotopes are also used in various PET applications.

Radiotracers are administered intravenously, with distribution throughout the body and detected by a PET detector, with average imaging sessions for preclinical PET of 10 to 60 minutes. Various protocols are designed and tailored for specific study aims, and the time points can vary from seconds to days after radiotracer administration. Dynamic protocols can be used to record multiple time points within a single scan. PET is employed for imaging of various conditions such as cancer, neurodegenerative disorders, and inflammation.

SPECT imaging is similar to traditional scintigraphy, which utilizes radioligands incorporating gamma-emitting radioisotopes (^{99m}Tc, ^{125}I, ^{111}In). A gamma-camera is fixed on a gantry (rotating frame) in a SPECT imaging machine, and a bed with the anesthetized animal is moved into location for imaging. The gamma-camera rotates around the subject and multiple cross-sectional images (projections) are acquired, which are then processed into a 3D image. Collimators are used to remove "noise" of gamma-rays and improve image quality with some decrease in sensitivity.

Nuclear imaging studies require a dedicated team comprised of a chemist to synthesize the specific radiotracer for the target of interest, a phlebotomist to deliver the tracer intravenously (usually IV tail vein), and a PET or SPECT technician to perform the scan and reconstruct the raw data. Reconstruction tools are usually provided along with acquisition software, and once reconstruction parameters are preset, typically the reconstruction process can run without further operator control. Reconstructed files can be opened by the investigator and analyzed in their laboratory with appropriate software, such as AMIDE[41] or DICOM[42] software packages. When a custom-made ligand is used, it is generally recommended to also perform a biodistribution study before planning imaging experiments to evaluate tissue and organ distribution of the ligand using a scintillation counter to quantify radioactivity in organs collected at necropsy.

Advantages

Nuclear studies, unlike most other imaging modalities, allow for time-related information regarding distribution and metabolism of biomolecules of interest such as the binding and distribution of an antibody-drug conjugate.[43] Functional changes often precede anatomical changes, and PET and SPECT are able to detect such molecular changes[44,45] as well as transient functional responses to pharmacological interventions. Nuclear imaging offers high sensitivity and can detect molecules at nanomolar and femtomolar levels.

Limitations

Nuclear imaging has poor anatomical localization, so CT or MRI scans are often performed and fused with PET or SPECT images to provide an anatomical reference to the functional imaging of PET or SPECT.[46,47] The short half-life of some isotopes (^{11}C, ^{18}F) requires scheduled coordination to make sure that all the animals, treatments, and personnel are ready for the study when the radiotracer is delivered. Working with radioactivity, there

are safety concerns, although with proper organization and safety protocols in place the nuclear studies are considered safe. Animals injected with isotopes need to be housed in special racks separated from the regular animal housing and housed separately until sufficient decay (10 half-lives, when about 99.9% of radioactive material is decayed, and it is generally considered safe to handle [by safety policies] fecal material or urine). If postimaging necropsy for gross anatomy and histological correlation is planned, the pathologist needs to take precautions against exposure to radioactive materials, especially in the case with longer-lived radioisotopes such as ^{111}In (half-life 2.81 days) or ^{125}I (half-life 60 days). Also, the availability of certain radioisotopes may depend on whether a cyclotron is located on-site for production of short-lived isotopes like ^{11}C, ^{18}F. Most major hospitals have cyclotrons for medical imaging use in patients.

Histopathological assessment may be important for the tracer uptake demonstration in tissues, for example, cancer metastases or small organs such as lymph nodes that are not easily identified by gross pathology. Another important consideration is that ^{18}F-FDG does not always identify all tumors. Histology-supporting studies allow for the identification of these variances from the norm.[48] Histological verification is accomplished by sampling organs (which match to reconstructed nuclear images)[48,49] and placing organs in formalin fixative, with a delay before histology processing to allow for radioactive decay. On the other hand, if the equipment is dedicated for the usage of radioactive tissues, careful processing of tissues can be done for histology in addition to biodistribution studies. This is a crucial aspect to include in nuclear imaging studies since poor resolution is a disadvantage in nuclear imaging. Yet, to remedy this problem, comparison of images with histopathology will undoubtedly add translational relevance to preclinical nuclear imaging studies since the tissue source of radioactivity that produced the reconstructed image needs to be correctly identified. Trained veterinary pathologists are experts in anatomy and pathology of multiple species and can easily assist scientists with this task.

Autoradiography is another way that radiotracers can be localized in organs such as bone,[50] heart,[51] and brain.[52] Nuclear imaging is always paired with MRI or CT for anatomical reference points for the nuclear scans to make localization of organs for histology or biodistribution demonstration.

Small vs Large Animal Imaging

Clinical PET systems designed for human patients are used for imaging large animals, both for veterinary and research purposes. Miniaturized high-sensitivity PET[53] and SPECT[54,55] scanners for preclinical imaging in small rodents are available in many institutions but require some capital for purchase and maintenance. Portable small PET scanners for imaging brain function for awake small rats in motion have been developed.[56]

Comparison of in vivo Nuclear Imaging to Pathology

Cardiac cell death can be monitored in the rat model of doxorubicin-induced cardiotoxicity using SPECT imaging.[57] Doxorubicin has been known for decades to induce acute and long-latency cardiac toxicity side effects due to cancer therapy. Multiple studies have been performed to investigate novel preventive, diagnostic, and treatment options to protect the cancer patients from anthracycline doxorubicin during cancer therapy. One of the challenges of preclinical studies directed against doxorubicin-induced cardiotoxicity is in determining a reliable method for evaluation of cell death due to doxorubicin treatment, especially important in evaluating potential cardioprotective drugs.[58,59] One method tested by several groups is SPECT imaging using ^{99m}Tc-labeled Annexin V[57,60]. Annexin binds to phosphatidylserine, which is a cell membrane component that is normally hidden in the cellular membrane but becomes exposed externally in dying cells. In Figure 3, SPECT imaging displayed increased uptake of radiolabeled Annexin V in the hearts of treated versus control rats. The increased cardiac cell death, induced by doxorubicin in this model, was further confirmed with terminal deoxynucleotidyl transferase dUTP nick-end labeling (TUNEL)-staining of cardiac tissue in a confirmation of cell death seen with SPECT imaging (see Figure 3).

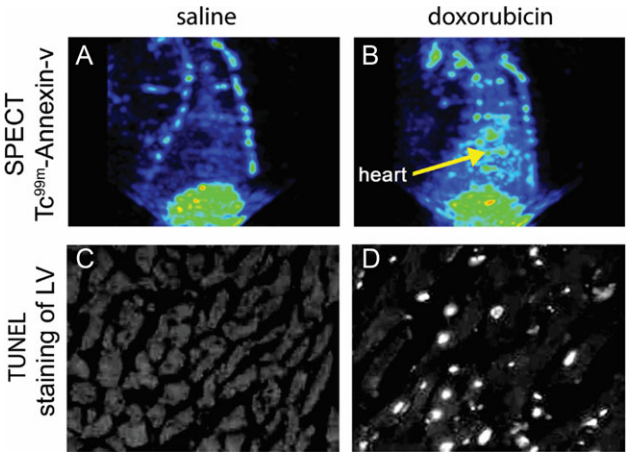

Figure 3 Single-photon emission computed tomography (SPECT) imaging of cell death in the rat heart. Rats were treated with doxorubicin at 2.5 mg/kg once a week for 6 weeks. Rats were injected with ^{99m}Tc-HYNIC-Annexin V. Relative to a SPECT image of the thorax of a saline control rat (A), SPECT images from a doxorubicin-treated rat (B) show increased uptake of radiolabeled annexin (arrow) in the heart. The extent of cardiac cell death in TUNEL tissue sections converted to black/white from saline control (C) and doxorubicin-treated rats (D). White nuclei indicate TUNEL-stained apoptotic nuclei. TUNEL staining correlated and supported the information supplied by SPECT, indicating that SPECT imaging is a useful noninvasive means of identifying cell death in vivo. LV = left ventricle. Maronpot et al. with permission.[6]

In an example of PET imaging in a Sinclair swine melanoma model, preclinical use of a novel targeted imaging agent, ^{124}I-cRGDY-PEG-C-dots, and comparison to a conventional nontargeted radiotracer, ^{18}F-FDG, was performed (Figure 4).[61] The novel agent was found to detect metastatic melanoma with high specificity, while the traditional tracer resulted in false positive findings caused by inflammatory lesions, as the increased metabolism it detects is not unique to neoplasia. These important findings were made possible by careful comparison of imaging and histopathology of multiple anatomical sites.

Summary

PET and SPECT require anatomical reference points that can be delivered by CT and MRI imaging. Sensitivity is high in nuclear imaging and nanomolar and femtomolar levels of detection can be achieved. Although widely used to identify tumors, ^{18}F-FDG may not always identify all metastatic disease and other methods may be clinically and preclinically needed.

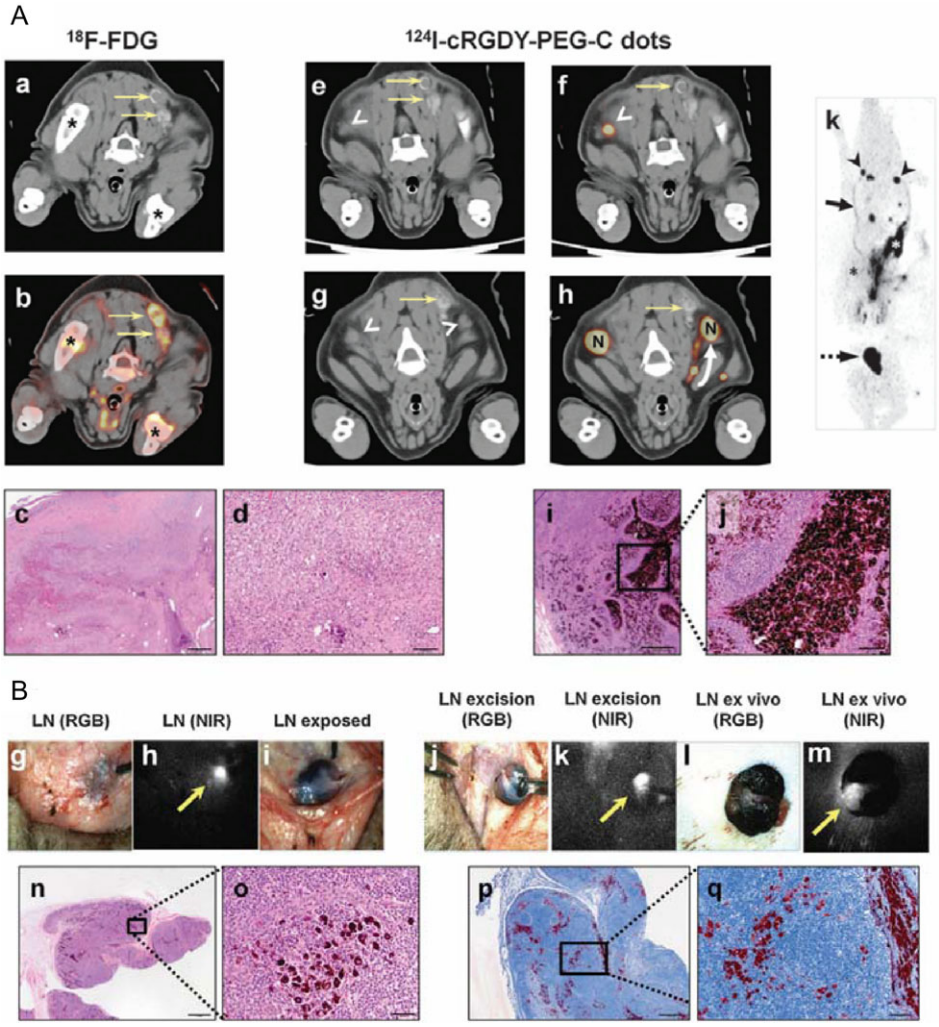

Figure 4 Swine model of melanoma positron emission tomography (PET) and optical imaging with pathology verification. (A) In a Sinclair swine model of melanoma, a novel targeted nanoparticle PET tracer, ^{124}I-cRGDY-PEG-C-dots, was compared with a conventional nontargeted tracer, ^{18}F-FDG. The former uses cRGDY peptide for targeting of integrin expressing tumors, while ^{18}F-FDG relies on the detection of enhanced glucose metabolism, a process that occurs in neoplastic tissue but may also detect other processes such as inflammation. (a) On fused PET/CT images, hypermetabolic foci were detected in calcified lymph nodes in the neck (yellow arrows) and bone marrow (black asterisks), and histopathology revealed chronic lymphadenitis with calcification but no evidence of neoplasia (c,d). Bone marrow uptake was attributed to high hematopoietic activity. In the same animal, after injection of targeted tracer ^{124}I-cRGDY-PEG-C-dots (e–h), no activity was detected in the calcified nodes (yellow arrows) or bone marrow, but PET-avid enlarged nodes were detected (N) as well as lymphatic drainage (white curved arrow), and these nodes were confirmed to contained metastatic melanoma on histopathology (i,j). ^{18}F-FDG failed to detect metastatic disease. Single frame from a 3-dimensional (3D) PET image reconstruction shows multiple bilateral metastatic nodes (arrowheads) and lymphatic channels (solid arrow) draining injection site (white asterisk) (k). Bladder activity is seen (dashed arrow). (B) The ^{124}I-cRGDY-PEG-C-dots also contained Cy5.5, a near-infrared organic dye, which allowed their use for real-time intraoperative visualization of sentinel lymph node (g–m). Histopathology confirmed correlation between optical signal and presence of metastatic melanoma in lymph nodes (n,o, H&E; p,q, immunohistochemistry for HMB45 melanocyte marker). Bradbury et al. with permission.[61]

CT and X-Ray Planar Radiography Modality

Background

X-ray imaging has been used in clinical settings and preclinical studies for decades. CT (computed tomography) is based on obtaining a series of X-ray-derived images (slices or projections) through the body, with subsequent reconstruction of the images resulting in a 3D image. X-ray source and a detector array fixed on a gantry rotate around the animal placed in a bed with attached anesthesia line. Many CT machines are built into a SPECT or PET machine and can be used independently of the nuclear imaging. Depending on X-ray absorbance by tissues with different densities and composition, the beam that exits the tissue varies in intensity and is quantified. The measure of X-ray attenuation is expressed in Hounsfield units. Radiopaque tissues, such as bone, appear white, air appears black, and soft tissues are seen as various shades of gray. The projection raw images are reconstructed to produce a 3D volume, and every resulting voxel (volume element) is assigned Hounsfield units by the CT scanner software.

A less expensive, simpler alternative to CT is planar radiography, which uses X rays to produce a 2D image of single projection of the subject. Planar radiography does not provide a 3D image but often generates sufficient information for the

purpose of the study, while being less time-consuming, less expensive, and requiring less sophisticated equipment and lower radiation exposure than CT imaging. Planar radiography is accomplished using tabletop cabinet X-ray equipment (eg, manufactured by Faxitron) that offers planar radiography specifically for small animals such as mice, rats, even marmosets[62] useful for multiple applications. Clinical veterinary or human planar radiograph equipment can be used for larger animal species.

Advantages

CT imaging time is relatively short (few minutes) and CT has relatively high spatial resolution.[63,64] Planar radiography x-ray imaging requires less time (15–60 seconds), and planar images are a composite of the various levels seen in CT. Machines are readily available at most institutions.

Limitations

CT and planar radiography imaging both require anesthesia of the animal to limit animal movement. In CT, x-ray exposure is higher than in planar x-ray examination, although advancements in CT imaging, such as helical scanning and multidetector CT systems, minimize the exposure. In CT, attenuation by tissues may limit the depth of penetration and requires attenuation correction algorithms. Since imaging is performed in living animals, the motion artifacts (breathing movements, beating heart) require additional corrections. Gating technique is used to extract images taken during selected parts of the movement cycle (eg, only during cardiac diastole).[65] Soft tissue resolution is not excellent, but contrast agents in small animals can be introduced to aid in soft tissue imaging.

Small vs Large Animal X-Ray Imaging

These methods have been available for all species for decades. Clinical machines are used for larger laboratory animals (nonhuman primates) or companion animals. One of the least expensive methods and easy to use and interpret, CT and planar radiography are both practical and applied to a range of species of animals.

Comparison of CT/X-Ray in Vivo Imaging to Pathology

Figure 5 illustrates an example of CT imaging after focal ablation by vascular-targeted photodynamic therapy of the porcine kidney. The goal of the study was to assess efficacy and safety of the procedure and the ability of CT imaging to document the ablation zone after treatment.[66] Post-ablation CT was performed and followed by histopathology. For histology, the kidney was carefully sectioned in the same location and plane as CT, and oversized cassettes and slides (5.5 × 4.5 cm) were used to maintain whole organ integrity to provide precise CT imaging to pathology correlation.

As another use of the CT imaging, osteosarcoma in bone can be imaged with CT, and the multiple views of the limb can determine the bone remodeling and invasion extent of the cancer. For example, the extent of bone reabsorption and bone formation induced by an osteosarcoma is exemplified in Figure 6. The tibia of a juvenile Sprague Dawley rat was implanted with 150,000 UMR106 rat osteosarcoma cells, and 3 weeks later a CT evaluation was performed. Reconstruction of

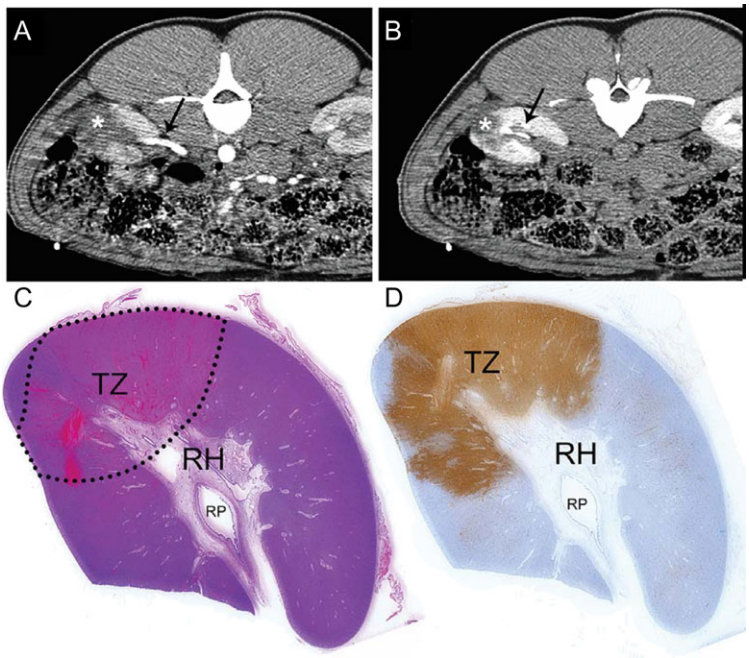

Figure 5 Renal ablation of the porcine kidney. CT imaging and histopathology of swine kidney after ablation by vascular-targeted photodynamic therapy. (A) Axial contrast-enhanced (by administration of iopamidol) CT scan obtained in the arterial phase to assess blood flow and vascular structures shows the treatment zone as a nonenhanced region of the right kidney (*) caused by decreased perfusion associated with necrosis. The right renal artery (arrow) was intact, patent, and without thrombosis, despite its proximity to the renal ablation. (B) Axial contrast-enhanced CT scan obtained in the delayed urographic phase to increase visualization of the renal collecting system (RCS) shows an intact RCS (arrow) and urinary excretion of contrast material without leakage. The treatment zone appears as a nonenhancing region of the right kidney, denoted by an asterisk (*). (C) Photomicrograph of a H&E-stained slide from the same kidney harvested 24 hours after ablation. The dotted line delineates the treatment zone (TZ), which includes the renal hilum (RH) and renal pelvis (RP). The treatment area is composed of necrotic renal tissues, with congestion and hemorrhage. (D) Terminal deoxynucleotidyl transferase dUTP nick-end labeling (TUNEL)-stained section confirms well-demarcated cell death in the ablated TZ at 24 hours posttreatment. Adapted from Kimm et al. with permission.[66]

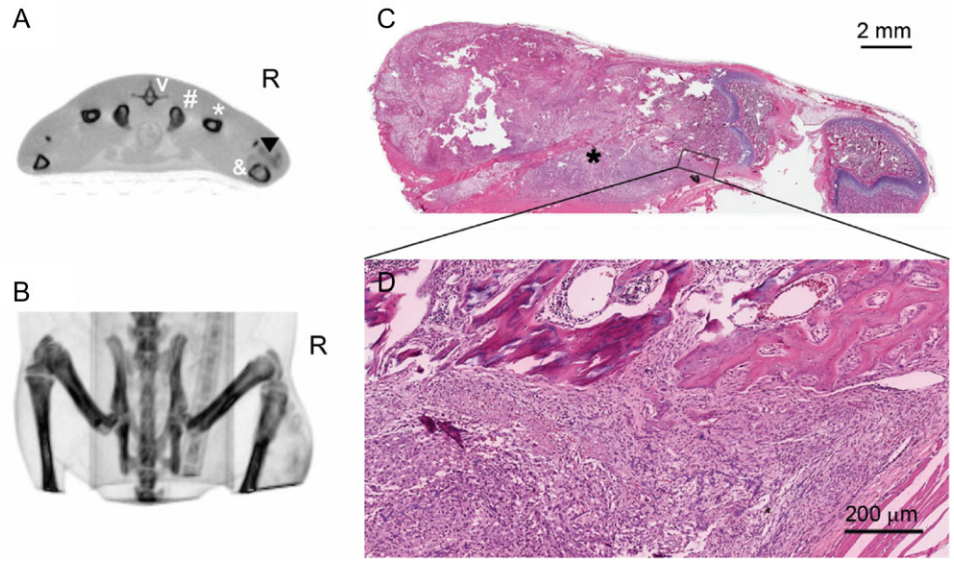

Figure 6 Computerized tomography (CT) imaging of rat osteosarcoma detects extent of bone invasion of tibia. (A) CT slice of a rat with an osteosarcoma in the right tibia (2 views with white and black reserved). V, vertebra; #, pelvis; *, femur; &, tibia (affected); ▼, osteosarcoma spreading to the soft tissues. (B) Three-dimensional (3D) rendering of right tibial osteosarcoma with comparison of unaffected left limb bone cortical disruption is noted. (C) The limb was amputated, decalcified, and processed for histology. The hematoxylin and eosin (H&E)-stained slide of the limb was scanned by Aperio scanner with comparison to CT images with cancer extending into tissues around bone. The area in the box from (C) is enlarged on the scanned slide showing the osteosarcoma invasion into the surrounding area (D). (unpublished data).

multiple projections gave a rendering of the tumor extent, and these data can be used to assign rats to treatment groups. This is important because only tumors that are correctly placed within the bone microenvironment (not subcutaneously placed) will metastasize to the lung. Alteration of the bone cortex in this example was crucial to determine the extent of invasiveness of the cancer. Comparison of the CT or planar radiography images with histopathology confirmed the extent, invasiveness, and pathogenesis of the cancer.

An application of the planar radiography (faxitron) x-ray method is applied to a mouse model of hypertrophic cardiomyopathy, developed by overexpressing ErbB2 in the mouse heart.[67] ErbB2 transgenic mice developed significant cardiac hypertrophy, with heart weights 2- to 3-fold larger than in wild-type mice (Figure 7). Planar radiography offered by (Faxitron) tabletop units is inexpensive and very easy to operate using either mammography film or a digital system to acquire and store images. Planar radiography has been used to determine the presence of lung inflammation or lung cancer, while in limbs, planar radiography is useful for evaluating cancer, fractures, or metabolic bone disease.

Summary

CT imaging has wide applications in imaging inflammation, detecting cancer, and evaluating toxicities.[68–76] Comparative in vivo x-ray imaging methods with pathology correlation improves research outcomes by increasing study rigor, reproducibility, and translational relevance. CT imaging is more expensive compared with planar radiography imaging. If planar radiography is available, the lower expense, ease of operation, and interpretation make planar radiography more practical in some cases. It would be best to use both methods initially and decide which is best for each particular model. CT is used in most nuclear imaging systems to give anatomical detail, but some CT equipment may have better resolution than others:

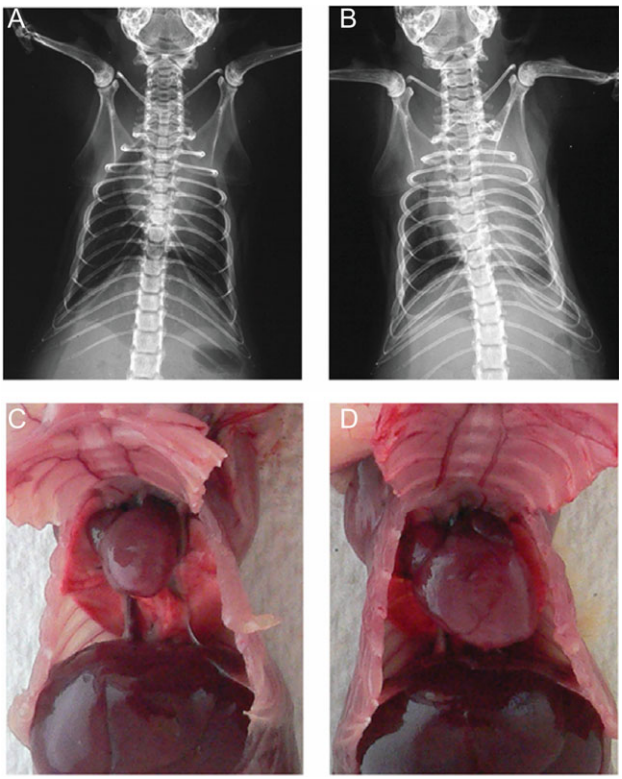

Figure 7 Planar radiography of the thorax with gross pathology correlation of the heart displays significant cardiac hypertrophy in ErbB2 transgenic mice. Eight- to 10-week-old mice were compared by planar radiography using faxitron machine. (A) Wild-type mice planar radiograph of thorax is compared with (B) ErbB2 transgenic mouse thorax to reveal enlarged cardiac silhouette in ErbB2 transgenic mouse. Wild-type mice (C) and ErbB2 transgenic mice (D) hearts in situ in thorax confirm the planar findings of enlarged atria and ventricles of the ErbB2 transgenic mouse. Sysa-Shah et al. with permission.[67]

for example, newer machines can detect 1-mm-sized pulmonary tumors by CT, but if those machines are not available, planar radiography may be a method of choice.

Optical Modality

Background

Optical imaging modalities are based on the detection of emitted light in the visible and near-infrared spectra. In biomedical research, well-established and widely used macroscopic optical imaging methods rely on light emitted by bioluminescence or fluorescence, but newer optical modalities taking advantage of other physical phenomena, such as Raman spectroscopy, have recently gained attention. Light detection for imaging purposes depends on highly sensitive charged-couple detectors, which are cryo-cooled to minimize noise generated by dark current, hence allowing detection of very low intensity light.[77]

Bioluminescence is the emission of light by living organisms as a result of a chemical reaction, a phenomenon that has been documented in many taxonomic groups. In the presence of the enzyme luciferase, the substrate luciferin is oxidized and photons are released. To harness this process for imaging purposes, genes coding for the luciferase from several organisms have been cloned and genetically engineered as reporters in cell lines and animals. The most commonly used luciferase is from the North American firefly (*Photinus pyralis*), but luciferases from other animal and bacterial species have also been cloned and used for imaging.[78,79] Unlike fluorescence, no external light source is required, but the luciferin substrate must be administered to mice by injection prior to imaging, which results in light emission for a limited period of time (10–20 minutes). Kinetics of bioluminescence is affected by the route of luciferin administration (intraperitoneal, subcutaneous, or intravenous), the organ or lesion being imaged, and the luciferase being used. Xenotransplantation of luciferase-transfected neoplastic cells into immunodeficient mice allows tracking of the cells in the entire body over time. In genetically engineered mice, the luciferase gene can be incorporated into constructs and driven by a ubiquitous or cell-specific promoters, allowing precise in vivo monitoring of biological phenomena in space and time.[80]

Fluorescence is the phenomenon by which some molecules, when exposed to light of an appropriate excitation wavelength, absorb photons and react by emitting photons of a longer wavelength. Fluorescent molecules (fluorophores) used for imaging purposes include fluorescent proteins that occur naturally in various organisms, such as the green fluorescent protein from the jellyfish *Aequorea victoria*, DsRed from the sea anemones *Discosoma spp*. and their variants,[81] and organic fluorescent dyes such as cyanine and xanthene derivatives. Quantum dots, a form of nanoparticles with intrinsic fluorescence, may also be used[78] although quantum dots can have potentially toxic cadmium metal cores. Genes for fluorescent proteins can be genetically engineered into model organisms and incorporated into proteins of interest as fusion proteins.[80] Fluorophores can also be conjugated to molecular probes incorporating ligands such as antibodies, which are administered prior to imaging. While in vivo bioluminescence and fluorescence can generally be imaged with the same equipment (a black chamber equipped with a charged-couple detector in which anesthetized mice are placed), the latter requires illumination of the animal and selection of appropriate filters corresponding to the excitation and emission spectra of the fluorophore.

Raman spectroscopy is a newer optical modality that presents significant advantages and opportunities. When matter is illuminated, most of the light is elastically scattered and retains its energy and wavelength (Rayleigh scattering), but a small fraction of the light is inelastically scattered with a lower energy and longer wavelength (the Raman effect). Because materials of different molecular composition inelastically scatter light differently, they have different Raman "signatures."[82,83] Raman spectroscopy is performed by illuminating a specimen and using a scattered light detector to characterize its Raman spectrum. Raman spectroscopy can be performed on cells and tissues without the use of probes, revealing their molecular composition as endogenous proteins and lipids produce distinct signatures, but it can also make use of probes that can be designed to target biological structures or functions. As the Raman effect is a very weak phenomenon in natural materials (a very small proportion of light is inelastically scattered), nanoparticles have been designed to enhanced intensity of the Raman phenomenon by several orders of magnitude (a strategy called surface enhanced Raman Scattering, SERS), thereby increasing sensitivity.[84]

Advantages

Optical modalities have several advantages over other imaging methods. Structures and functions of interest can be precisely targeted by the use molecular probes or genetic engineering that do not involved radionuclides, therefore increasing safety for the animals and for the research personnel performing imaging, as well as subsequent work on the animals such as husbandry, necropsy, and histology. Optical imaging has a high molecular sensitivity (the lowest amount of a probe that can be accurately detected), usually in the nanomolar range, which is comparable to nuclear modalities.[85] In some applications, SERS Raman spectroscopy has been reported to have a femtomolar sensitivity.[84] Compared with other imaging modalities, systems used to perform bioluminescence and fluorescent imaging are relatively inexpensive and easy to operate. Images acquisition is relatively fast (few second to minutes) and multiple mice can be imaged at the same time. The size of the files generated is small, and no complex postprocessing of the raw data is necessary to obtain usable images. For these reasons, optical imaging is well suited for high-throughout applications.

Limitations

As optical modalities rely on the detection of light, the ability of light to travel through tissues is a major limitation of these methods. Animals are shaved before imaging to increase the light or fluorescence signal and reduce autofluorescence, but even after the hair is removed, autofluorescence can still be a significant problem. As photons are absorbed and scattered by tissues, the intensity and spatial resolution are significantly affected, and this becomes more problematic when attempting to detect signal located deep within tissues. For fluorescence, fluorophores with a near-infrared emission spectrum are generally preferred as they have greater penetrance through tissues compared with fluorophores emitting shorter wavelengths such as green fluorescent protein.[78] While the small size of mice allows for optical imaging of internal organs, this is not possible in humans in which these modalities are limited to intraoperative and endoscopic applications; therefore, most of

the optical imaging procedures performed in mice are not translatable to humans. Autofluorescence of endogenous tissue components and of ingesta (alfalfa in food) within the gastrointestinal tract is a limitation of fluorescent imaging, as it reduces signal to background ratio; however, bioluminescence and Raman spectroscopy do not present this limitation. Duration of imaging is limited by photobleaching of fluorescent probes and by the brief bioluminescence period (10–20 minutes) following administration of luciferin, but Raman nanoprobes are not affected by such constraints. The availability of Raman spectroscopy as an in vivo imaging modality remains limited to specialized laboratories at this time.

Small vs Large Animal Imaging

As in humans, applications of optical imaging in large animals are limited to detection of targets on or near the surface of tissues, and imaging of internal organs is not possible except in intraoperative contexts. As such optical applications are being developed for human medicine, large animal models are being used to test their efficacy, for example in sentinel lymph node mapping,[61] but such translational studies are hampered by the limited availability of suitable large animal cancer models. In Figure 4, a Sinclair swine model of melanoma was used to assess the efficacy of a targeted imaging agent designed for intraoperative visualization of lymph node metastases by the surgeon. Histopathology of resected lymph nodes was performed to assess sensitivity and specificity of the imaging modality. As the recent emergence of genome editing by CRISPR-Cas9 allows easier genetic engineering of large animal species such as swine, and the reporter-gene imaging paradigm using fluorescent proteins has been applied in this species,[86] the use of optical in vivo imaging in large animal models may become more common.

Comparison of Optical Imaging to Pathology

Optical imaging offers the ability to examine the entire body of a mouse and detect with high sensitivity rare lesions with small size, such as micrometastases, while such lesions may be very difficult or impossible to efficiently detect by gross and histopathologic examination. However, after a lesion has been detected by imaging, careful histopathology performed on the organ of interest can provide greatly enhanced resolution and documentation. Therefore, optical imaging and histopathology are complimentary methods that offer the opportunity for comprehensive and powerful analyses when combined. Additionally, when an optical signal is targeted to a cell type or a lesion by the use of a promoter-driven reporter or a targeted probe, histopathology is the gold standard that may ultimately support the sensitivity and specificity of the targeting strategy. As antibodies reacting with luciferases, fluorescent proteins, or other probes component are available, precise visualization of the imaging signal at the level of tissues and cells, and correlation with histopathologic changes can be achieved on formalin-fixed paraffin embedded tissues. Fluorophores may also be detected directly by fluorescence microscopy, but this requires the use of frozen sections, as fluorescence is generally not preserved after formalin-fixed paraffin embedded processing. An example is provided in Figure 8, illustrating in vivo imaging and histopathology of genetically engineered mice in which a mutated gene of interest was conditionally expressed in germinal center B cells (GCBCs), a subset of lymphocytes, and firefly luciferase was included in the construct. In vivo imaging confirmed expression of the transgene in lymphoid organs, including the spleen, and histology and immunohistochemistry for luciferase confirmed the imaging finding but also provided the higher resolution required to confirm that the targeting strategy was successful, resulting in expression in GCBCs.

In an example of Raman spectroscopy imaging in Figure 9, surface enhanced resonance Raman scattering (an improvement of SERS in which the signal is amplified by resonance between the probe and incident detection laser) nanoparticles were used to detect pancreatic tumors at surgery in real time.[84] Precise correlation of imaging, macroscopic, and microscopic pathologic findings, as well as immunohistochemistry for the nanoparticles, demonstrated the excellent performance of this imaging strategy, which detected not only advanced neoplasms but also preneoplastic lesions.

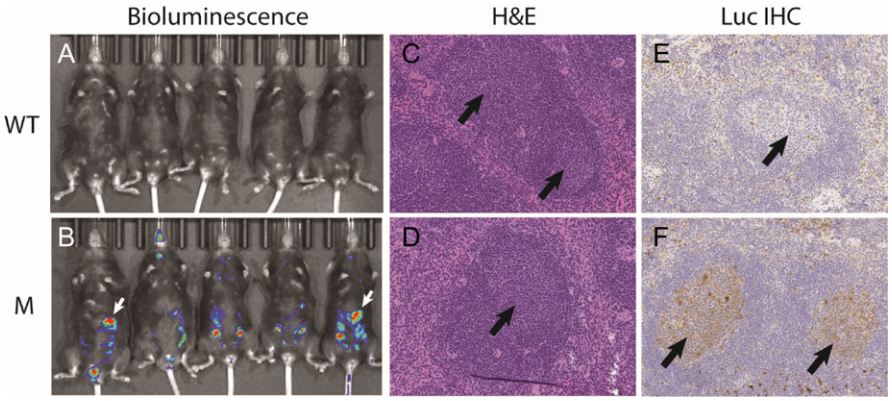

Figure 8 Optical imaging of mice detects lymphoid hyperplasia in germinal centers. To investigate the function of a gene of interest in a subset of lymphocytes, GCBCs, genetic engineering was performed to induce this mutation in this cell population. Mice were immunized to induce lymphoid hyperplasia with germinal center formation. The firefly luciferase reporter was incorporated in the mutant DNA construct to image its expression in the targeted B cells. (A) Wild-type mice without reporter and (B) mutant mice with imaging construct were compared. Bioluminescence signals were observed in mutant mice and the most intense signal (white arrows) corresponded to the spleen, with other foci of expression consistent with lymph nodes and intestinal Peyer's patches. On immunohistochemistry for luciferase on splenic sections, expression was located within GCBCs in mutant mice (black arrows, F), while no staining was observed in germinal centers of wild-type mice (E). (C,D) Hematoxylin and eosin (H&E)-stained sections confirming the presence of germinal centers in both genotypes. Luc IHC, luciferase immunohistochemistry; M, mutant; WT, wild type. (unpublished data).

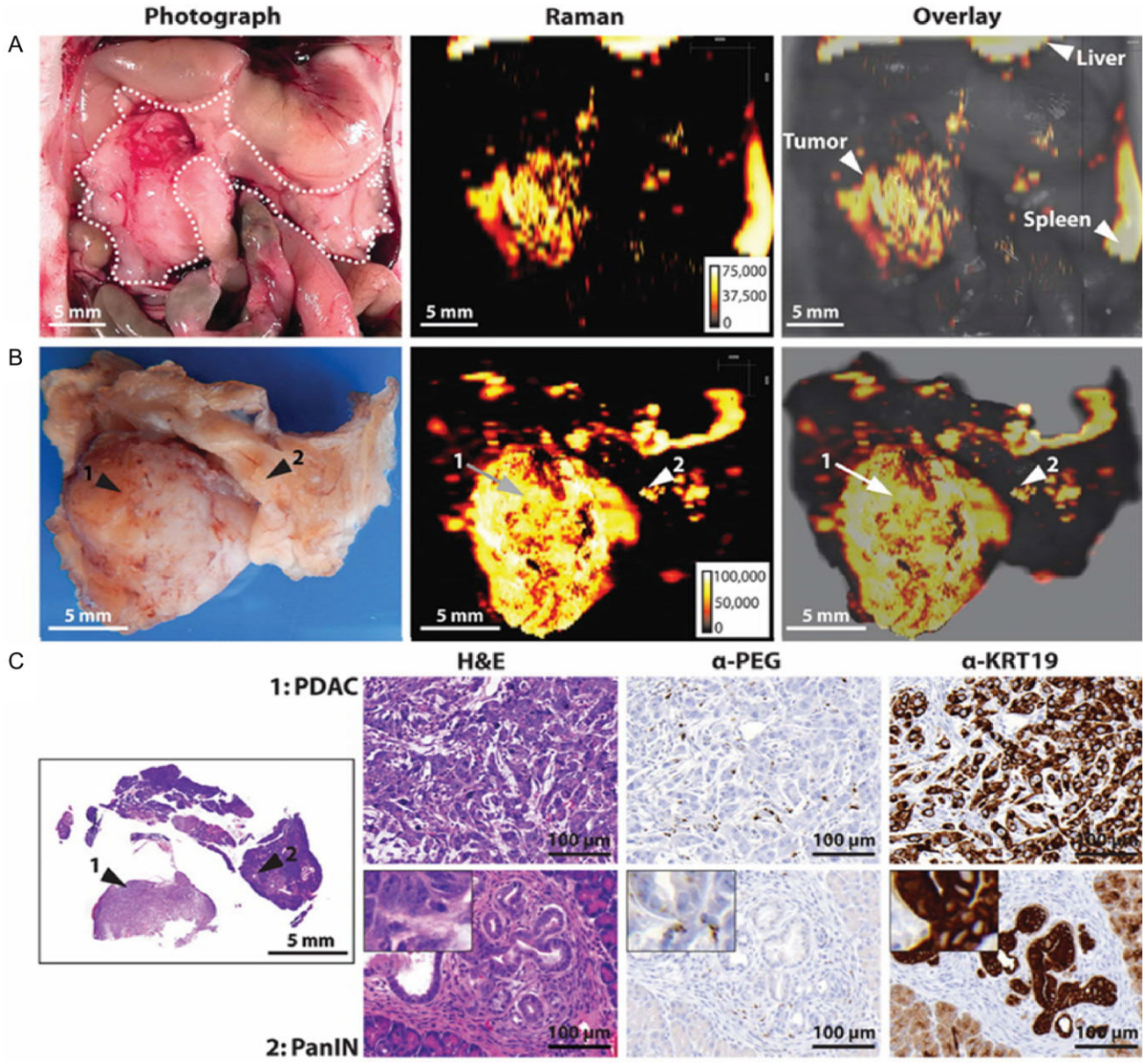

Figure 9 Surface enhanced resonance Raman scattering (SERRS) nanoparticles detect pancreatic tumors at surgery in real time. SERRS nanoparticles, designed for resonance in the near-infrared window, and conjugated with polyethylene glycol (PEG), were administered to mice with pancreatic ductal neoplasia as a proof of concept of their use as an intraoperative imaging agent. Imaging of the pancreas in situ (A) and ex vivo (B) revealed diffuse signal in a grossly visible tumor (arrows 1) and in multiple small foci in grossly normal pancreatic parenchyma (arrows 2), which corresponded to a pancreatic ductal adenocarcinoma (PDAC) and microscopic pancreatic intraepithelial neoplasia (PanIN) on histology, respectively, therefore confirming their high sensitivity for the detection of malignant and premalignant lesions. (C) Immunohistochemistry for PEG was used to detect particles and for cytokeratin 19 (KRT19) to enhance visualization of proliferative ductal lesions. Harmsen et al. with permission.[84]

Summary

Optical imaging is less expensive than MR and nuclear imaging and easier to perform and interpret compared with other imaging modalities. Optical imaging can be combined with other modalities, such as CT, to provide anatomical context. The increased sensitivity of these methods is an advantage and compares to nuclear imaging. Pairing optical imaging with comparative pathology will improve reproducibility and translational relevance by allowing for an additional imaging method to identify micrometastases that could be too small to see on a gross pathology exam during necropsy. In addition, the ability to image 3 to 5 animals at one time allows for a higher throughput for evaluation of the disease process.

MRI Modality

Background

Magnetic Resonance Imaging employs a powerful and uniform magnetic field and radio frequency (RF) energy and is based on the 2 properties of charged nuclear particles (protons): the constant angular momentum and a magnetic moment. The angular momentum and the magnetic moment, as vector entities, have directionality and spin (wobble) features. When placed in a strong magnetic field, the protons, which normally are randomly oriented, align either parallel or antiparallel to the magnetic field and absorb energy when aligned by a pulse from the MRI magnet coil. The nuclei return to their normal alignment

(relaxation), the absorbed energy is returned as RF pulses, and an additional gradient coil locates the X, Y, and Z orientation of the tissue magnetic resonance (MR) signal after each magnetic pulse. Various sequences of RF pulses (applied and collected), timing variations, and acquisition parameters can be designed, producing different types of images.

The hydrogen proton, ^{1}H, is the most commonly used nucleus for MRI since it is the most abundant atomic nucleus in the body. ^{1}H anatomic images are based on the hydrogen in tissue water and are dependent on ^{1}H concentration and polarization degree as well as its gyromagnetic properties. Other atomic nuclei (^{31}P, ^{13}C, ^{23}Na, ^{19}F, and $^{17}O_2$ as well as hyperpolarized nuclei such as helium) can be used for MRI. There are 2 main relaxation types: spin–lattice (longitudinal) and spin–spin (transverse) relaxations, and the images are produced based on tissue differences in the longitudinal (referred to as T1) and transverse (referred to as T2) relaxation times. By varying the timing parameters of RF pulses (pulse sequences), an acquired image can be either T1- or T2-weighted to enhance contrast of specific tissue pathologies. Gadolinium-based image contrast enhancement can be achieved by shortening T1 relaxation time to track blood flow following intravenous administration or to image the GI tract following oral administration.

Diverse MRI techniques are used for a multitude of preclinical and clinical purposes. MRI contrast agents or superparamagnetic nanoparticles allow evaluation of blood flow dynamics, oxygen status in areas of perfusion, tissue cellularity, areas of necrosis, and inflammation. Functional MRI can identify functional and dysfunctional areas in the brain based on an increase in oxygenated blood in areas of increased neural activity. Cardiac MRI is used to evaluate cardiac function in preclinical models of heart disease.[87,88] MRI is particularly advantageous in studying the soft tissue anatomy: resolutions of 25 to 100 μm are achievable in preclinical animal studies of cancer,[89] brain injury,[90] and stem cells.[91]

Advantages

MRI is a powerful, noninvasive method for phenotypical characterization and therapeutic efficacy evaluation in animal models of disease used in preclinical research and drug discovery and development. In vivo MRI provides an opportunity for longitudinal evaluation of tissue changes and phenotypic expression in experimental animal models to monitor progression, regression, and therapeutic responses noninvasively. Ex vivo MRI of fixed specimens allows a thorough examination of multiple digital slices while leaving the specimen intact for subsequent conventional histopathological evaluation of regions of interest.[92–95]

Limitations

The cost of equipment acquisition and transportation, operation, and maintenance for conventional MRI systems is relatively high, and thus specialized institutional facilities are necessary where these systems can be isolated for safety reasons. Recently, compact MRI systems have been developed that are designed for operation in conventional laboratories without the cost, complexity, and infrastructure of conventional MRI systems.[94,96]

Table 2 A comparison between the main characteristics of compact MRI and traditional superconducting MRI systems

	Permanent magnet compact MRI	Traditional superconducting MRI
Size	Compact	Not compact
Field strength	1 T	4.7–9.4 T
Resolution	Limited to 60 microns ex vivo and 100 microns in vivo	Down to 20 microns ex vivo and 30 microns in vivo
Scan time	Typical 5 minutes for in vivo	1 to 2 minutes for in vivo
Cryogenic operation of magnet	No	Yes
Price	Low (starts from 300 US$)	At least 3 times more
Upfront site preparations	Negligible	Significant
	No dedicated power supply, no RF shielded room, no cryogens	Infrastructure adaptations required (shielded/isolated room/water cooling/3 phase electricity/substantial HVAC)
Safety	Very safe	Restricted
	Practically no fringe field, allowing no restrictions with magnet location	Special attention is required. May have extensive 5 Gauss stray field
Siting and moving flexibility	Flexible	Limited flexibility
	The instrument is wheeled and can be easily moved	Support infrastructure may make it problematic to move
Animal handling for imaging	Instrument can be moved into animal facility	Animals must be removed from animal facility for imaging
Electricity and water cooling	Single-phase power outlet	Three-phase electricity
	No water cooling required	Cryogenic infrastructure; compressor and cryogens
Ongoing maintenance considerations and running costs	Negligible	Considerable
	Electronics can be switched off overnight for zero energy costs	System is ON 24/7. Cryogenic infrastructure must be periodically serviced
System operation	Routine operation, high throughput. Behind the barrier operation	Often requires MRI expertise
Advanced MRI protocols	Limited	Available
Acoustic noise	Negligible acoustic noise	Substantial (may require acoustic shielding)

MRI, magnetic resonance imaging; T, Tesla; US$, United States dollars; RF, radio frequency; HVAC, Heating, ventilation, and air conditioning.

Small vs Large Animal Imaging

Although examples below focus on imaging mice in research, clinical machines at medical centers are being used to image larger research subjects or companion animals. For example, MRI-guided biopsy of a vertebral body mass has been used to diagnose an osteosarcoma in a Rottweiler dog.[97] In laboratory experiments, MRI has been used to elucidate percutaneously accessible lymph nodes in pigs[98] for development of methods that can be translated to human medicine. Many veterinary schools have MRI capabilities on site or in collaboration with a local medical institution.

Comparison of MRI to Pathology

Information obtained from MRI is advantageous in obtaining accurate information such as location, volume, and number of the investigated lesions to the scientific team, including the pathologist involved in the process of determining product safety and drug efficacy in nonclinical settings.

MRI performed on a living animal is referred to as traditional in vivo MRI. When the MRI is performed on fixed specimens taken from a euthanized animal or biopsy, it is called ex vivo MRI.[96] The main advantage of the in vivo MRI is the ability to perform longitudinal assessments of changes in the target and adjacent tissues, thereby allowing to monitor progression, regression, and therapeutic effects in a noninvasive and nondestructive manner.[6] Such a method provides means to reduce the number of animals required for each study and to avoid the need for interim sacrifice of animals. The main advantage of the ex vivo MRI is the possibility to thoroughly examine the tissue of interest after it has been fixed in formalin but before the organ has been dissected and its orientation destroyed by the dissection process. After ex vivo MRI, the tissue

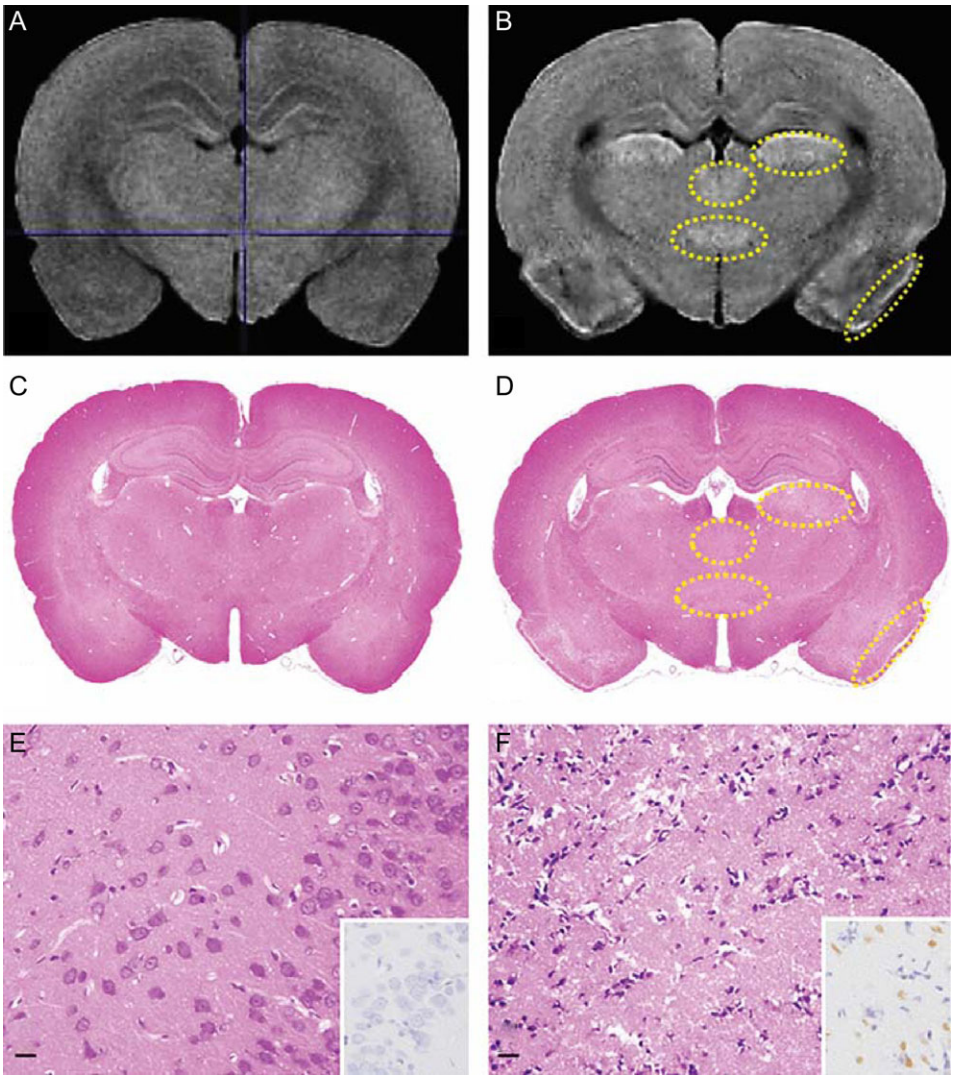

Figure 10 MRI detects brain necrosis in cortex and thalamus due to pilocarpine treatment to mice. MRI images (A,B), T1-weighted images, and comparative histology with hematoxylin and eosin (H&E) staining (C–F). The T1-weighted image of brain the pilocarpine-treated mice (B) showed high T1 signal areas (yellow dotted line regions) compared with the control animal (A). In the histology of the comparative cross section, the pilocarpine-treated mouse brain (D,F) exhibited pale areas in the piriform cortex and lateral thalamic nucleus compared to the control (C,E). Photos E and F are higher magnification of the piriform cortex. E is normal control. In F, there is widespread necrosis with neuronal loss. Lower bottom inset shows terminal deoxynucleotidyl transferase dUTP nick-end labeled (TUNEL)-positive apoptotic cells in F (brown nuclear staining), while TUNEL-staining is negative in the inset of photo E. Taketa T, et al. with permission.[102]

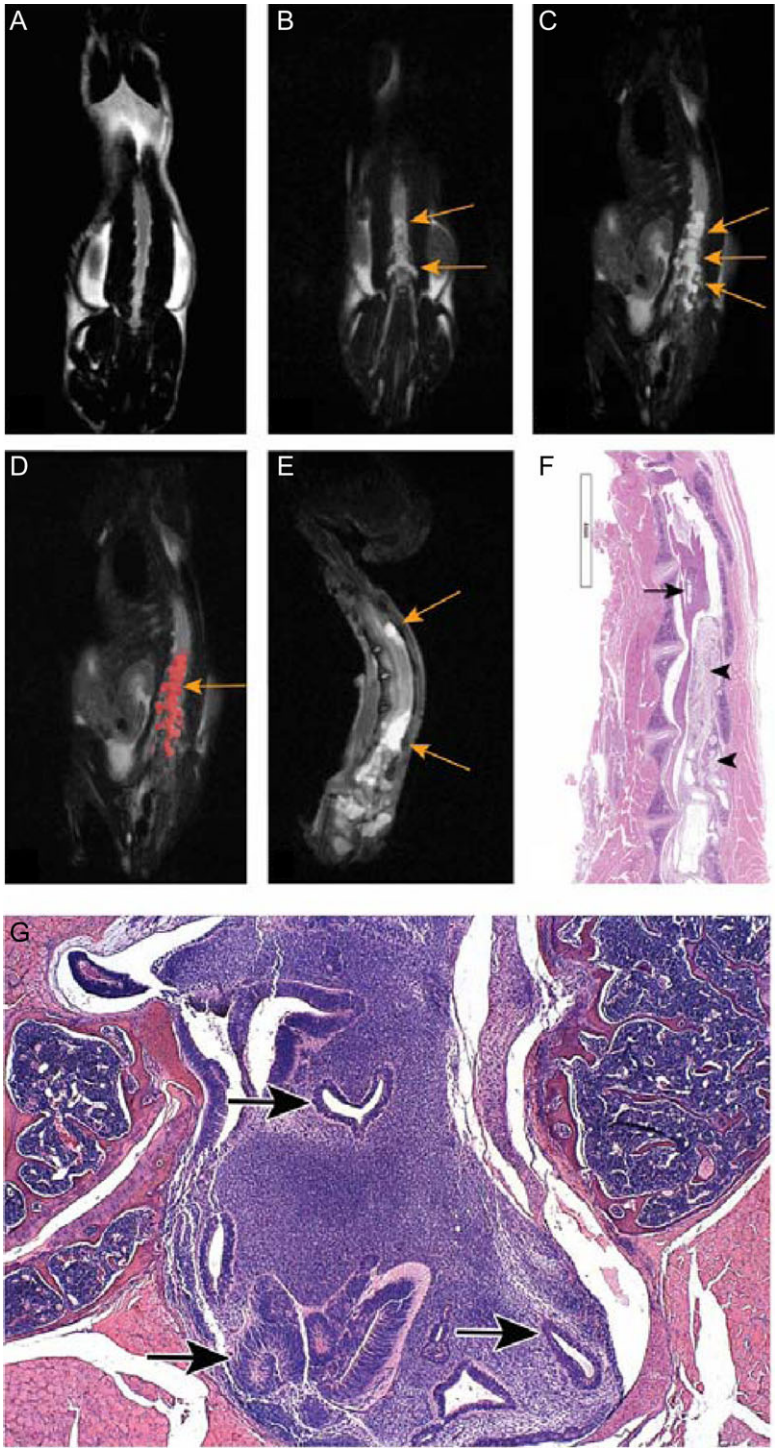

Figure 11 MRI detects a teratoma invading the vertebra in a mouse. In vivo coronal view (A) of a control animal. In vivo coronal view (B–D) and ex vivo sagittal view (E) of MRI of the spinal cord of a NOD-SCID (NOD.CB17-Prkdcscid/NCrHsd) mouse 25 days (B) and 48 (C–E) days after intrathecal injection of hESCs. Note the bright lesion (arrows) located in the lumbar regions, which expanded from day 25 to 48. Intensity-based segmentation (D) allowed for quantitative assessment of the lesion and the region of interest was found to have a volume of 82.62 μL and confirmed by histology as an invasive teratoma (F; arrow, teratoma invading the spinal cord; arrowheads, teratoma invading the vertebra and compressing the spinal cord). MRI acquisition parameters: In vivo (B–D): fast spin echo, TE 80 ms; TR 2400 ms; slice thickness 1 mm; field of view 70 mm; matrix size 200 ×192; acquisition time 5.5 min ex vivo (E): fast spin echo, TE 74 ms; TR 3000 ms; slice thickness 0.7 mm; field of view 45 mm; matrix size 256 × 250; acquisition time 63 min. (G) Higher magnification hematoxylin and eosin (H&E)-stained slide (x40) of the teratoma invading into the spinal cord. Note (arrows) structures suggesting primitive neuroectodermal tissue, consisting of neural-tube and rosette-like structures. Ramot et al. with permission.[93]

stays intact and can be used for conventional histopathology evaluation, which can be better directed based on the results of the MRI images. Furthermore, ex vivo MRI scans can also provide important information on the structure and volume of the lesions,while also providing information on the effects on adjacent, seemingly unaffected tissue.[6,92–94,96]

Until recently, MRI was underutilized in preclinical toxicity testing, mainly because conventional MRI systems had several inherent limitations, including high costs and safety concerns. Therefore, such imaging machines could only be utilized by large research centers. The advent of new compact MRI systems has solved these past issues with MRI. These imaging machines are relatively inexpensive, self-contained and self-shielded, and are movable. These characteristics make the compact MRI systems possible to use by almost all laboratories or research facilities. Table 2 provides a comparison between compact MRI systems and traditional superconducting MRI systems. The compact MRI system has several additional advantages on conventional MRI systems, including quicker scanning times; no need for cryogenic operation of magnet, dedicated power supply, water cooling, or RF shielded room; and negligible acoustic noise. Furthermore, in addition to being less expensive to purchase than the conventional MRI systems, compact MRI systems are much more economical in terms of operation and maintenance costs.[94] All these advantages place the MRI as one of the leading imaging modalities for preclinical testing, and the growing number of models that have been tested with this modality increase its validity as an adjunctive tool for preclinical assessments. Nevertheless, it is still necessary that the regulatory agencies provide guidance for use of all imaging modality data, including MRI.[6]

Compact MRI use in ex vivo and in vivo preclinical models is advantageous to use with histopathology since some organs such as the brain are very heterogeneous, and it is not possible to histologically section and review every region completely. Compact MRI on a fixed brain can inform the pathologist where to sample and perform histologic evaluation.

In Figure 10, compact MRI and histopathology are combined for neurotoxicity testing. The traditional neurotoxicologic approach of selecting 7 brain sections in rodents[99,100] is significantly improved by the application of compact MRI, assisting in the localization of lesions likely missed on the 7 cutting planes that are traditionally sectioned in whole brains.[101] The obvious advantage is that MRI scans can provide the equivalent of 64 coronal sections comparable to transverse sections of histopathology. The use of MRI can also allow each animal to serve as its own control if imaged before treatment.

When considering stem cell clinical applications, there are regulatory requirements for preclinical assessments that include testing for potential induction of tumors[103] due to stem cells. In Figure 11 MRI examination revealed abnormal pale areas in the spinal cord and brain, which correlated histopathologically to a teratoma. This study shows the efficacy of compact MRI systems in the detection of a small teratoma following intrathecal injection of hESCs in a highly sensitive manner, with acquisition times of 5.5 minutes in vivo and 61 to 63 minutes ex vivo.

In addition to the above-mentioned example, the compact MRI has already been shown to be of benefit for quantifying the volume of preneoplastic changes in liver and kidney carcinogenesis models.[96] MRI can be used for following the growth of local tumors, thus enabling determination between benign tumors and fast-growing malignant lesions.[104] The fact that MRI can cover the whole body of the animal enables the evaluation of the effects of tumors on adjacent tissues and the overall systemic condition of the animal. The addition of specific contrast agents can also give functional information regarding tumors. Such methods, in addition to dynamic contrast-enhanced MRI, for example, can be used for real-time follow-up of the therapeutic effects of different anti-cancer treatments.[105] Based on the accumulating information on the utility of MRI and compact MRI systems for the detection and volume measurements of preneoplastic and neoplastic changes, it is evident that in vivo and ex vivo MRI can be applied to carcinogenicity studies.

Summary

Practical MRI for use in investigative and preclinical toxicology studies is now feasible. Newly developed, self-containing imaging systems provide an efficient and cost-effective means to rapidly obtain in vivo and ex vivo MRI images to support the hypothesis-driven research.

Conclusions

Despite significant advances in technologies available to scientists for evaluation of animal models, pathology remains a gold standard for a complete analysis of the outcome of an animal model study. Coupled with longitudinal in vivo imaging methods, candidate drug targets such as oncogenes or other disease drivers can be demonstrated, and drugs in development can be easily tested for efficacy as well as toxicity. Both approaches offer different but complementary scientific data. This combined approach can reduce the numbers of animals needed for study and thus reduce time and costs needed to meet the scientific goals of the project. Using both longitudinal imaging paired with gross and histopathology of the animals at the end of the study will improve the scientific significance and the reproducibility of experimental data. This combined methodology (in vivo imaging and pathology) will ultimately decipher biological questions and significantly translate findings of animal studies for application of human medicine outcomes in a logical and practical approach to rapidly increase the pace of novel scientific discoveries for meaningful translational relevance.

Acknowledgments

We thank Dr. Hal Dietz and his lab and Dr. David Huso for images of the Marfan mice in Figure 2. We thank Drs. Ari Melnick and Yanwen Jiang for their contribution in designing the genetically engineered mouse strain shown in Figure 8.

Financial support. KG was supported in part by American Heart Association 15GRNT25760029 and National Institutes of Health (HL088649, CA204345, CA209884, CA204555, CA229582). SM was supported in part by Cancer Center Support Grant P30 CA008748. CM was supported by the Lymphoma Research Foundation.

Potential conflicts of interest. All authors: No reported conflicts.

References

1. Jaaro-Peled H, Niwa M, Foss CA, et al. Subcortical dopaminergic deficits in a DISC1 mutant model: a study in direct reference to human molecular brain imaging. *Hum Mol Genet*. 2013;22(8):1574–1580.
2. Lee JS, Orita H, Gabrielson K, et al. FDG-PET for pharmacodynamic assessment of the fatty acid synthase inhibitor C75 in an experimental model of lung cancer. *Pharm Res*. 2007;24(6):1202–1207.
3. Diogo R, Molnar J. Links between evolution, development, human anatomy, pathology, and medicine, with a proposition of a re-defined anatomical position and notes on constraints and morphological "imperfections". *J Exp Zool B Mol Dev Evol*. 2016;326(4):215–224.

4. Cunha L, Horvath I, Ferreira S, et al. Preclinical imaging: an essential ally in modern biosciences. *Mol Diagn Ther*. 2014; 18(2):153–173.
5. Lauber DT, Fulop A, Kovacs T, Szigeti K, Mathe D, Szijarto A. State of the art in vivo imaging techniques for laboratory animals. *Lab Anim*. 2017;51(5):465–478.
6. Maronpot RR, Nyska A, Troth SP, et al. Regulatory forum opinion piece*: imaging applications in toxicologic pathology-recommendations for use in regulated nonclinical toxicity studies. *Toxicol Pathol*. 2017;45(4):444–471.
7. Peterson RA, Gabrielson KL, Allan Johnson G, Pomper MG, Coatney RW, Winkelmann CT. Continuing education course #1: non-invasive imaging as a problem-solving tool and translational biomarker strategy in toxicologic pathology. *Toxicol Pathol*. 2011;39(1):267–272.
8. Zanzonico P. 2017. Noninvasive imaging for supporting basic research. In: Kiessling F, Pichler BJ, Hauff P, eds. Small Animal Imaging. 2nd ed. Cham, Germany: Springer International Publishing. p. 3–32.
9. Wang LW, Huttner IG, Santiago CF, et al. Standardized echocardiographic assessment of cardiac function in normal adult zebrafish and heart disease models. *Dis Model Mech*. 2017;10(1):63–76.
10. Flores LE, Hildebrandt TB, Kuhl AA, Drews B. Early detection and staging of spontaneous embryo resorption by ultrasound biomicroscopy in murine pregnancy. *Reprod Biol Endocrinol*. 2014;12:38.
11. Peavey MC, Reynolds CL, Szwarc MM, et al. A novel use of three-dimensional high-frequency ultrasonography for early pregnancy characterization in the mouse. *J Vis Exp*. 2017;128.
12. Peavey MC, Reynolds CL, Szwarc MM, et al. Three-dimensional high-frequency ultrasonography for early detection and characterization of embryo implantation site development in the mouse. *PLoS One*. 2017;12(1): e0169312.
13. Foster FS, Brown AS. Microultrasound and its application to longitudinal studies of mouse eye development and disease. *Cold Spring Harb Protoc*. 2012;2012(4):494–503.
14. Pierfelice TJ, Gaiano N. Ultrasound-guided microinjection into the mouse forebrain in utero at E9.5. *J Vis Exp*. 2010;45.
15. Zlitni A, Yin M, Janzen N, et al. Development of prostate specific membrane antigen targeted ultrasound microbubbles using bioorthogonal chemistry. *PLoS One*. 2017;12(5):e0176958.
16. Denbeigh JM, Nixon BA, Hudson JM, Puri MC, Foster FS. VEGFR2-targeted molecular imaging in the mouse embryo: an alternative to the tumor model. *Ultrasound Med Biol*. 2014;40(2):389–399.
17. Denbeigh JM, Nixon BA, Puri MC, Foster FS. Contrast imaging in mouse embryos using high-frequency ultrasound. *J Vis Exp*. 2015;97.
18. Kiessling F, Fokong S, Koczera P, Lederle W, Lammers T. Ultrasound microbubbles for molecular diagnosis, therapy, and theranostics. *J Nucl Med*. 2012;53(3):345–348.
19. Needles A, Heinmiller A, Sun J, et al. Development and initial application of a fully integrated photoacoustic micro-ultrasound system. *IEEE Trans Ultrason Ferroelectr Freq Control*. 2013;60(5):888–897.
20. Lindsey BD, Shelton SE, Foster FS, Dayton PA. Assessment of molecular acoustic angiography for combined microvascular and molecular imaging in preclinical tumor models. *Mol Imaging Biol*. 2017;19(2):194–202.
21. Lindsey BD, Shelton SE, Martin KH, et al. High resolution ultrasound superharmonic perfusion imaging: in vivo feasibility and quantification of dynamic contrast-enhanced acoustic angiography. *Ann Biomed Eng*. 2017;45 (4):939–948.
22. Shelton SE, Lindsey BD, Tsuruta JK, Foster FS, Dayton PA. Molecular acoustic angiography: a new technique for high-resolution superharmonic ultrasound molecular imaging. *Ultrasound Med Biol*. 2016;42(3):769–781.
23. Hoyt K, Warram JM, Wang D, Ratnayaka S, Traylor A, Agarwal A. Molecular ultrasound imaging of tissue inflammation using an animal model of acute kidney injury. *Mol Imaging Biol*. 2015;17(6):786–792.
24. Lee HJ, Hwang SI, Byun J, Kong HY, Jung HS, Kang M. Ultrasound contrast-enhanced study as an imaging biomarker for anti-cancer drug treatment: preliminary study with paclitaxel in a xenograft mouse tumor model (secondary publication). *Ultrasonography*. 2017;36(4):370–377.
25. Ma YY, Jin KT, Wang SB, et al. Molecular imaging of cancer with nanoparticle-based theranostic probes. *Contrast Media Mol Imaging*. 2017;2017:1026270.
26. Murphy HW, Dennis P, Devlin W, Meehan T, Kutinsky I. Echocardiographic parameters of captive western lowland gorillas (Gorilla gorilla gorilla). *J Zoo Wildl Med*. 2011;42(4):572–579.
27. Vinhas M, Araujo AC, Ribeiro S, Rosario LB, Belo JA. Transthoracic echocardiography reference values in juvenile and adult 129/Sv mice. *Cardiovasc Ultrasound*. 2013;11:12.
28. Sysa-Shah P, Tocchetti CG, Gupta M, et al. Bidirectional cross-regulation between ErbB2 and beta-adrenergic signalling pathways. *Cardiovasc Res*. 2016;109(3):358–373.
29. Bauer M, Cheng S, Jain M, et al. Echocardiographic speckle-tracking based strain imaging for rapid cardiovascular phenotyping in mice. *Circ Res*. 2011;108(8):908–916.
30. Kovacs A, Olah A, Lux A, et al. Strain and strain rate by speckle-tracking echocardiography correlate with pressure-volume loop-derived contractility indices in a rat model of athlete's heart. *Am J Physiol Heart Circ Physiol*. 2015;308(7):H743–H748.
31. Shepherd DL, Nichols CE, Croston TL, et al. Early detection of cardiac dysfunction in the type 1 diabetic heart using speckle-tracking based strain imaging. *J Mol Cell Cardiol*. 2016;90:74–83.
32. Heyne GW, Plisch EH, Melberg CG, Sandgren EP, Peter JA, Lipinski RJ. A simple and reliable method for early pregnancy detection in inbred mice. *J Am Assoc Lab Anim Sci*. 2015;54(4):368–371.
33. Barkley MS, Geschwind II, Bradford GE.The gestational pattern of estradiol, testosterone and progesterone secretion in selected strains of mice. *Biol Reprod*. 1979;20(4):733–738.
34. Pallares P, Fernandez-Valle ME, Gonzalez-Bulnes A. In vivo virtual histology of mouse embryogenesis by ultrasound biomicroscopy and magnetic resonance imaging. *Reprod Fertil Dev*. 2009;21(2):283–292.
35. Ng CM, Cheng A, Myers LA, et al. TGF-beta-dependent pathogenesis of mitral valve prolapse in a mouse model of Marfan syndrome. *J Clin Invest*. 2004;114(11):1586–1592.
36. Habashi JP, Judge DP, Holm TM, et al. Losartan, an AT1 antagonist, prevents aortic aneurysm in a mouse model of Marfan syndrome. *Science*. 2006;312(5770):117–121.
37. Pachon RE, Scharf BA, Vatner DE, Vatner SF. Best anesthetics for assessing left ventricular systolic function by echocardiography in mice. *Am J Physiol Heart Circ Physiol*. 2015;308(12):H1525–H1529.
38. Yao R, Lecomte R, Crawford ES. Small-animal PET: what is it, and why do we need it? *J Nucl Med Technol*. 2012;40(3): 157–165.

39. Vaquero JJ, Kinahan P. Positron emission tomography: current challenges and opportunities for technological advances in clinical and preclinical imaging systems. *Annu Rev Biomed Eng*. 2015;17:385–414.
40. Khalil MM, Tremoleda JL, Bayomy TB, Gsell W. Molecular SPECT imaging: an overview. *Int J Mol Imaging*. 2011;2011: 796025.
41. Loening AM, Gambhir SS. AMIDE: a free software tool for multimodality medical image analysis. *Mol Imaging*. 2003; 2(3):131–137.
42. Digital Imaging and Communications in Medicine (DICOM). *NEMA Publications PS 3.1–1998*. Rosslyn, VA: National Electrical Manufacturers Association; 1998.
43. ter Weele EJ, Terwisscha van Scheltinga AG, Kosterink JG, et al. Imaging the distribution of an antibody-drug conjugate constituent targeting mesothelin with (8)(9)Zr and IRDye 800CW in mice bearing human pancreatic tumor xenografts. *Oncotarget*. 2015;6(39):42081–42090.
44. Bernsen MR, Vaissier PE, Van Holen R, Booij J, Beekman FJ, de Jong M. The role of preclinical SPECT in oncological and neurological research in combination with either CT or MRI. *Eur J Nucl Med Mol Imaging*. 2014;41(Suppl 1): S36–S49.
45. Franc BL, Acton PD, Mari C, Hasegawa BH. Small-animal SPECT and SPECT/CT: important tools for preclinical investigation. *J Nucl Med*. 2008;49(10):1651–1663.
46. Chatziioannou AF. Instrumentation for molecular imaging in preclinical research: Micro-PET and Micro-SPECT. *Proc Am Thorac Soc*. 2005;2(6):533–536, 510–511.
47. Shao Y, Cherry SR, Farahani K, et al. Simultaneous PET and MR imaging. *Phys Med Biol*. 1997;42(10):1965–1970.
48. Bhatnagar A, Wang Y, Mease RC, et al. AEG-1 promoter-mediated imaging of prostate cancer. *Cancer Res*. 2014;74 (20):5772–5781.
49. Bhang HE, Gabrielson KL, Laterra J, Fisher PB, Pomper MG. Tumor-specific imaging through progression elevated gene-3 promoter-driven gene expression. *Nat Med*. 2011;17 (1):123–129.
50. Phulpin B, Dolivet G, Marie PY, et al. Re-assessment of chronic radio-induced tissue damage in a rat hindlimb model. *Exp Ther Med*. 2010;1(4):553–560.
51. Tran N, Poussier S, Franken PR, et al. Feasibility of in vivo dual-energy myocardial SPECT for monitoring the distribution of transplanted cells in relation to the infarction site. *Eur J Nucl Med Mol Imaging*. 2006;33(6):709–715.
52. Sharp FR, Evans K. Regional (14C) 2-deoxyglucose uptake during vibrissae movements evoked by rat motor cortex stimulation. *J Comp Neurol*. 1982;208(3):255–287.
53. Moses WW. Fundamental limits of spatial resolution in PET. *Nucl Instrum Methods Phys Res A*. 2011;648(Supplement 1):S236–S240.
54. Scherfler C, Donnemiller E, Schocke M, et al. Evaluation of striatal dopamine transporter function in rats by in vivo beta-[123I]CIT pinhole SPECT. *Neuroimage*. 2002; 17(1):128–141.
55. van der Have F, Vastenhouw B, Ramakers RM, et al. U-SPECT-II: an ultra-high-resolution device for molecular small-animal imaging. *J Nucl Med*. 2009;50(4):599–605.
56. Schulz D, Southekal S, Junnarkar SS, et al. Simultaneous assessment of rodent behavior and neurochemistry using a miniature positron emission tomograph. *Nat Methods*. 2011;8(4):347–352.
57. Gabrielson KL, Mok GS, Nimmagadda S, et al. Detection of dose response in chronic doxorubicin-mediated cell death with cardiac technetium 99m annexin V single-photon emission computed tomography. *Mol Imaging*. 2008;7(3):132–138.
58. Gabrielson K, Bedja D, Pin S, et al. Heat shock protein 90 and ErbB2 in the cardiac response to doxorubicin injury. *Cancer Res*. 2007;67(4):1436–1441.
59. Sysa-Shah P, Xu Y, Guo X, et al. Geranylgeranylacetone blocks doxorubicin-induced cardiac toxicity and reduces cancer cell growth and invasion through RHO pathway inhibition. *Mol Cancer Ther*. 2014;13(7):1717–1728.
60. Bennink RJ, van den Hoff MJ, van Hemert FJ, et al. Annexin V imaging of acute doxorubicin cardiotoxicity (apoptosis) in rats. *J Nucl Med*. 2004;45(5):842–848.
61. Bradbury MS, Phillips E, Montero PH, et al. Clinically-translated silica nanoparticles as dual-modality cancer-targeted probes for image-guided surgery and interventions. *Integr Biol (Camb)*. 2013;5(1):74–86.
62. Olson EJ, Shaw GC, Hutchinson EK, et al. Bone disease in the common marmoset: radiographic and histological findings. *Vet Pathol*. 2015;52(5):883–893.
63. Lombardi CM, Zambelli V, Botta G, et al. Postmortem microcomputed tomography (micro-CT) of small fetuses and hearts. *Ultrasound Obstet Gynecol*. 2014;44(5):600–609.
64. Rueckel J, Stockmar M, Pfeiffer F, Herzen J. Spatial resolution characterization of a X-ray microCT system. *Appl Radiat Isot*. 2014;94:230–234.
65. Badea C, Hedlund LW, Johnson GA. Micro-CT with respiratory and cardiac gating. *Med Phys*. 2004;31(12):3324–3329.
66. Kimm SY, Tarin TV, Monette S, et al. Nonthermal ablation by using intravascular oxygen radical generation with WST11: dynamic tissue effects and implications for focal therapy. *Radiology*. 2016;281(1):109–118.
67. Sysa-Shah P, Xu Y, Guo X, et al. Cardiac-specific overexpression of epidermal growth factor receptor 2 (ErbB2) induces pro-survival pathways and hypertrophic cardiomyopathy in mice. *PLoS One*. 2012;7(8):e42805.
68. Ashton JR, West JL, Badea CT. In vivo small animal micro-CT using nanoparticle contrast agents. *Front Pharmacol*. 2015;6:256.
69. Badea CT, Fubara B, Hedlund LW, Johnson GA. 4-D micro-CT of the mouse heart. *Mol Imaging*. 2005;4(2):110–116.
70. Brown RH, Irvin CG, Allen GB 3rd, et al. An official ATS conference proceedings: advances in small-animal imaging application to lung pathophysiology. *Proc Am Thorac Soc*. 2008;5(5):591–600.
71. Cavanaugh D, Johnson E, Price RE, Kurie J, Travis EL, Cody DD. In vivo respiratory-gated micro-CT imaging in small-animal oncology models. *Mol Imaging*. 2004;3(1):55–62.
72. Martiniova L, Schimel D, Lai EW, Limpuangthip A, Kvetnansky R, Pacak K. In vivo micro-CT imaging of liver lesions in small animal models. *Methods*. 2010;50(1):20–25.
73. Solomon HM, Makris SL, Alsaid H, et al. Micro-CT imaging: developing criteria for examining fetal skeletons in regulatory developmental toxicology studies—a workshop report. *Regul Toxicol Pharmacol*. 2016;77:100–108.
74. van Deel E, Ridwan Y, van Vliet JN, Belenkov S, Essers J. In vivo quantitative assessment of myocardial structure, function, perfusion and viability using cardiac micro-computed tomography. *J Vis Exp*. 2016;108:53603.
75. Vasquez SX, Shah N, Hoberman AM. Small animal imaging and examination by micro-CT. *Methods Mol Biol*. 2013;947: 223–231.
76. Wise LD, Xue D, Winkelmann CT. Micro-computed tomographic evaluation of fetal skeletal changes induced by all-

trans-retinoic acid in rats and rabbits. *Birth Defects Res B Dev Reprod Toxicol*. 2010;89(5):408–417.
77. Moomaw B. Camera technologies for low light imaging: overview and relative advantages. *Methods Cell Biol*. 2013; 114:243–283.
78. Alves F, Bode J, Cimalla P, et al. 2017. Optical imaging, Chapter 16. In Kiessling F, Hauff P, eds. *Small Animal Imaging*. 2nd ed. Cham, Germany: Springer International Publishingr. p. 403–490.
79. Hastings JW. Chemistries and colors of bioluminescent reactions: a review. *Gene*. 1996;173(1 Spec No):5–11.
80. Herschman HR. Noninvasive imaging of reporter gene expression in living subjects. *Adv Cancer Res*. 2004;92:29–80.
81. Day RN, Davidson MW. The fluorescent protein palette: tools for cellular imaging. *Chem Soc Rev*. 2009;38(10):2887–2921.
82. Andreou C, Kishore SA, Kircher MF. Surface-enhanced raman spectroscopy: a new modality for cancer imaging. *J Nucl Med*. 2015;56(9):1295–1299.
83. Winnard Jr. PT, Zhang C, Vesuna F, et al. Organ-specific isogenic metastatic breast cancer cell lines exhibit distinct Raman spectral signatures and metabolomes. *Oncotarget*. 2017;8(12):20266–20287.
84. Harmsen S, Huang R, Wall MA, et al. Surface-enhanced resonance Raman scattering nanostars for high-precision cancer imaging. *Sci Transl Med*. 2015;7(271):271ra277.
85. Tichauer KM, Wang Y, Pogue BW, Liu JT. Quantitative in vivo cell-surface receptor imaging in oncology: kinetic modeling and paired-agent principles from nuclear medicine and optical imaging. *Phys Med Biol*. 2015;60(14): R239–R269.
86. Ruan J, Li H, Xu K, et al. Highly efficient CRISPR/Cas9-mediated transgene knockin at the H11 locus in pigs. *Sci Rep*. 2015;5:14253.
87. Santer D, Nagel F, Kreibich M, et al. In vivo and ex vivo functional characterization of left ventricular remodelling after myocardial infarction in mice. *ESC Heart Fail*. 2015;2 (3):171–177.
88. Messner NM, Zollner FG, Kalayciyan R, Schad LR. Preclinical functional magnetic resonance imaging part ii: the heart. *Z Med Phys*. 2014;24(4):307–322.
89. Raman V, Pathak AP, Glunde K, Artemov D, Bhujwalla ZM. Magnetic resonance imaging and spectroscopy of transgenic models of cancer. *NMR Biomed*. 2007;20(3):186–199.
90. Ngen EJ, Wang L, Gandhi N, et al. A preclinical murine model for the early detection of radiation-induced brain injury using magnetic resonance imaging and behavioral tests for learning and memory: with applications for the evaluation of possible stem cell imaging agents and therapies. *J Neurooncol*. 2016;128(2):225–233.
91. Ngen EJ, Wang L, Kato Y, et al. Imaging transplanted stem cells in real time using an MRI dual-contrast method. *Sci Rep*. 2015;5:13628.
92. Nyska A, Schiffenbauer YS, Brami CT, Maronpot RR, Ramot Y. Histopathology of biodegradable polymers: challenges in interpretation and the use of a novel compact MRI for biocompatibility evaluation. *Polym Advan Technol*. 2014;25(5): 461–467.
93. Ramot Y, Schiffenbauer YS, Amouyal N, et al. Compact MRI for the detection of teratoma development following intrathecal human embryonic stem cell injection in NOD-SCID mice. *Neurotoxicology*. 2017;59:27–32.
94. Ramot Y, Schiffenbauer YS, Maronpot R, Nyska A. Compact magnetic resonance imaging systems-novel cost-effective tools for preclinical drug safety and efficacy evaluation. *Toxicol Sci*. 2017;157(1):3–7.
95. Tempel-Brami C, Pinkas I, Scherz A, Salomon Y. Detection of light images by simple tissues as visualized by photosensitized magnetic resonance imaging. *PLoS One*. 2007;2(11): e1191.
96. Tempel-Brami C, Schiffenbauer YS, Nyska A, et al. Practical applications of in vivo and ex vivo MRI in toxicologic pathology using a novel high-performance compact MRI system. *Toxicol Pathol*. 2015;43(5):633–650.
97. Krimins RA, Fritz J, Gainsburg LA, et al. Use of magnetic resonance imaging-guided biopsy of a vertebral body mass to diagnose osteosarcoma in a Rottweiler. *J Am Vet Med Assoc*. 2017;250(7):779–784.
98. Kraitchman D, Kamel I, Weiss C, Georgiades C. Elucidation of percutaneously accessible lymph nodes in swine: a large animal model for interventional lymphatic research. *J Vasc Interv Radiol*. 2017;28(3):451–456.
99. Bolon B, Garman RH, Pardo ID, et al. STP position paper: recommended practices for sampling and processing the nervous system (brain, spinal cord, nerve, and eye) during nonclinical general toxicity studies. *Toxicol Pathol*. 2013;41 (7):1028–1048.
100. Rao DB, Little PB, Malarkey DE, Herbert RA, Sills RC. Histopathological evaluation of the nervous system in National Toxicology Program rodent studies: a modified approach. *Toxicol Pathol*. 2011;39(3):463–470.
101. Hanig J, Paule MG, Ramu J, et al. The use of MRI to assist the section selections for classical pathology assessment of neurotoxicity. *Regul Toxicol Pharmacol*. 2014;70(3):641–647.
102. Taketa Y, Shiotani M, Tsuru Y, et al. Application of a compact magnetic resonance imaging system for toxicologic pathology: evaluation of lithium-pilocarpine-induced rat brain lesions. *J Toxicol Pathol*. 2015;28(4):217–224.
103. Cunningham JJ, Ulbright TM, Pera MF, Looijenga LH. Lessons from human teratomas to guide development of safe stem cell therapies. *Nat Biotechnol*. 2012;30(9): 849–857.
104. Liu Y, Yin T, Feng Y, et al. Mammalian models of chemically induced primary malignancies exploitable for imaging-based preclinical theragnostic research. *Quant Imaging Med Surg*. 2015;5(5):708–729.
105. Wang H, Marchal G, Ni Y. Multiparametric MRI biomarkers for measuring vascular disrupting effect on cancer. *World J Radiol*. 2011;3(1):1–16.